

Application of Foil Bearings to Helium Turbocompressor

Dr. H. Ming Chen
Senior Staff Specialist
Foster-Miller Technologies
431 New Karner Road
Albany, NY 12205
518-456-9919, x104
mchen@fosmiltech.com

Dr. Roy Howarth
Consultant
13 Longview Drive
Clifton Park, NY 12065
518-371-6322
royhowarth@mindspring.com

Mr. Bernard Geren
Vice President
Turbotechnology Services
8 Sarnowski Drive
Scotia, NY 12302
518-372-2496
tscbernie@hotmail.com

Mr. Jay C. Theilacker
Fermi National Accelerator Laboratory
Mail Stop 347
P.O. Box 500
Batavia, IL 60510
630-840-3238
theilacker@fnal.gov

Mr. William M. Soyars
Fermi National Accelerator Laboratory
Mail Stop 347
P.O. Box 500
Batavia, IL 60510
630-840-3362
soyars@fnal.gov

SYNOPSIS

Hydrodynamic gas-lubricated foil bearings are ideal for machinery that operates at high speed or in extreme-temperature environments. This paper presents an application example of the successful replacement of a tape-type bearing for a bump-type bearing in a helium turbocompressor.

Dr. H. Ming Chen, a graduate of National Taiwan University and Rensselaer Polytechnic Institute, is a senior staff specialist at Foster-Miller Technologies (FMT) in Albany, New York. Prior to joining FMT, he was the Vice President of Engineering and cofounder of Mohawk Innovative Technology. Dr. Chen has more than 25 years of experience in the design of innovative rotor-bearing systems. During his tenure with Mechanical Technology Inc., he led the technology development of the world's largest active magnetic bearing system. His current research focuses on the development of foil gas bearings for high-speed turbomachinery and hybrid magnetic bearings for blood pumps and momentum energy-storage flywheel systems. He is a member of ASME and a registered professional engineer in the state of New York.

Dr. Roy Howarth graduated in mechanical engineering from the University of Manchester, England, and was subsequently awarded his M.Sc., by the same institution, in 1960 for his work on the application of automatic control to hydrostatic bearings. After working in the aircraft industry, he joined the faculty of the University of Salford, England, as Professor of Mechanical Engineering, where he worked mainly in the fields of fluid mechanics and tribology. During his tenure at the University of Salford, he was awarded a Ph.D. for his work in tribology. In 1979, Dr. Howarth moved to the United States to work at Mechanical Technology Inc. (MTI) where he remained until 1998. At MTI, he was involved in research and development efforts in the tribology field and rotating machinery troubleshooting. Dr. Howarth is now an independent consultant.

Bernard Geren is a vice president and cofounder of Turbotechonology Services Corporation (TSC) of Scotia, New York, where he is responsible for the design of new centrifugal compressors and aftermarket components, as well as modifications and rerating of existing compressor designs. He received his B.S.M.E. degree from Union College and has over 30 years of experience in the design, testing, and troubleshooting of centrifugal compressors and high-speed machinery, gained from various positions held with Mechanical Technology Inc., Turbonetics, and Atlas Copco Comptec.

ABSTRACT

Hydrodynamic gas-lubricated foil bearings are ideal for machinery that operates at high speed or in extreme-temperature environments. As motors and generators run at higher speeds with more torque capacity, the need for commonly available, robust, high-speed, low-loss foil bearings is clear. This paper presents an application example of the successful replacement of a tape-type bearing for a bump-type bearing in a helium turbocompressor. Both bearing types are described, as are the steps involved in design and fabrication of the bump bearing, and results of comparison tests between the original and replacement bearings. Methods to analyze bump-type foil bearings with commercially available software are reviewed to further emphasize the inherent simplicity of these bearings. By providing the engineering community with the understanding needed to successfully apply foil bearings, the authors hope that the benefits and true potential of this technology will finally be realized.

INTRODUCTION

Research on high-speed foil bearings has been performed since the early 1970s. This early work resulted in the development of various designs of foil bearings (see Figure 1), such as bump type (Gray, et al., 1981; Heshmat, et al., 1983; Ku and Heshmat, 1997), leaf type (Agrawal, 1997; San Andres, 1995; Oh and Rhode, 1976), and tape type (Licht, et al., 1981). Among these three, the bump type has been the most publicized and popular. Gray's paper documents the design methodology for bump-type bearings, and addresses issues involving materials and coatings, manufacturing procedure, fabrication accuracy effect, misalignment, Coulomb damping, shock tolerance, dynamic stability, analytical tools, and so forth. However, two decades later, although there are an increasing number of potential applications for foil bearings, such as microturbines, they have yet to become off-the-shelf items (see Figure 2). In fact, initial development costs remain unreasonably high for new applications, with a common perception of many in the industry that foil bearing design remains a "black art." With motors and generators running at higher and higher speeds and increased torque capacity, the need for a robust, high-speed, low-loss foil bearing design is clear. For example, permanent-magnet brushless motors can directly drive a 300-hp compressor at 70,000 rpm. At these speeds, rolling-element bearings have delicate lubrication problems or limited service life. Active magnetic bearings may be too expensive or have touchdown bearing problems. In these and many similar applications, foil bearings offer distinct advantages when they can be produced reliably in large quantities.

This paper presents a successful retrofit of bump-type radial bearings for a helium turbocompressor (see Figure 3). The original bearings were tape-type bearings that had suffered service life problems due to external vibrations (Soyars and Fuerst, 2000). We focused on a simple but robust bump bearing configuration. Analyses included methods needed to determine gas film properties, heat transfer, foil bump stress, stiffness and Coulomb damping, and rotor-bearing dynamics. The fabrication process is outlined, and bump making, heat treatment, tack welding, and quality issues are reviewed. Finally, test results are summarized and compared to predictions.

ORIGINAL BEARING DESIGN

The helium compressor consists of a single-stage impeller powered by a variable frequency induction motor with an operating speed of 40,000 to 90,000 rpm. The vertical rotor in the compressor weighs about 1.2 lb. The rotor is supported radially by two identical tape-type foil bearings and axially by a spiral-groove, gimbal-mounted gas thrust bearing. The latter worked adequately and is not discussed further. Each radial bearing consists of one strip of foil

(Figure 4) which, when coiled up and placed in the housing (with the correct shim thickness) forms three complete coils (Figure 5). The one-piece strip has three sections:

- An outer coil, 0.002-in. thick and divided into 12 equal-length segments by shallowly etched grooves.
- A middle coil, about 0.015-in. thick, also divided into 12 equal-length segments by shallow grooves. This segment of the foil has a sandy outside surface, which promotes friction between it and the outer coil.
- An inner coil, 0.002-in. thick and divided into 4 equal-length segments by shallow axial grooves. These segments are curved to conform to the final ID of the bearing, and have Teflon-coated bearing surfaces.

As shown in Figure 5, each segment of the outer and middle coils spans 30° and the segments lie on top of each other. The segments of the inner foil each span 90° and are supported on the middle and outer segments, which act as leaf springs. This essentially forms a four-lobe bearing. The dimension between the two opposite segments is smaller than the shaft diameter. When the shaft is installed, the outer and middle segments are displaced radially by 0.010 in. Treating each segment as a beam with built-in ends, the combined stiffness of the outer and middle foils is 90 lb/in. so that, under static conditions, each segment applies a radial load to the shaft of 0.90 lb (preload). Under static conditions, the clearance between the outer foil segments and the housing is about 0.0014 in. The overall bearing stiffness is 540 lb/in. (= 6 x 90, with the 6 factor being derived from the geometry of the 12 even segments, each spanning 30°). With this stiffness, the outer foils would contact the housing if a static load of 0.75 lb were applied to the bearing. This amounts to 2.2 psi for the bearing diameter of 0.63 in. and length of 0.54 in. In the authors' experience, a foil bearing should be designed for a load of 20 psi or more at operating speed. The very low 2.2-psi load capacity of the original bearings explains their limited service life.

Although the original bearing had low load-carrying capability, there was no reported history or evidence of subsynchronous whirl problems, an indication that the bearings had good damping properties. We estimated the amount of Coulomb damping present as follows:

$$E = 6\mu F_0 \Delta$$

where E = vibration energy dissipated by frictional force

μ = frictional coefficient

Δ = small journal displacement

F_0 = preload = 0.9 lb.

For $\mu = 0.1$ and $\Delta = 0.001$ -in, an equivalent viscous damping would be:

$$B = 4E/\pi\omega\Delta^2 = 24\mu F_0/\pi\omega\Delta \text{ lb-sec/in.}, \text{ then } \omega B = 24\mu F_0/\pi\Delta = 688 \text{ lb/in.}$$

where ω = vibration frequency in rad/sec. With similar values for bearing damping ($\omega B = 688$ lb/in.) and stiffness ($K = 540$ lb/in.), we concluded that the bearing had adequate damping.

It should be emphasized that the estimation of foil bearing damping based on energy dissipation is an engineering design "gauge," and is by no means rigorous. Indeed, it was clearly shown

theoretically by Vance and San Andres (1999) that pure Coulomb damping would result in infinite vibration amplitude at the critical speed. Some other types of damping must exist in foil bearings, such as hysteresis damping as reported by Ku and Heshmat (1993).

To understand how the rotor behaved in the bearings, an undamped critical speed analysis was performed with the results presented in Figures 6, 7, and 8. The results show two low rigid-body critical speeds (one translational mode and one conical mode) with large displacements at the bearings. This is an encouraging sign for a well-behaved system if the bearings themselves possess damping.

REPLACEMENT BEARING DESIGN

The fundamental construction of a bump-type radial foil bearing consists of two thin strips of foil. The top or inner foil is smooth and supported by a bump foil consisting of uniformly spaced, cylindrically shaped bumps, which have been preformed into the foil. The bearing is unidirectional, with the shaft rotating from free end to fixed end of the top foil. It is a hydrodynamic bearing, operable with a film of gas, liquid, or a mix of both. Its ability to conform and comply removes the necessity of maintaining the high degree of dimensional accuracy and roundness normally required in rigid surface bearings.

In operation, both the foils deflect under the hydrodynamic pressure generated between the journal and top foil. As the bump foil deflects, the bumps are also displaced circumferentially. The relative motions between the bump foil and top foil, and between the bump foil and bearing housing introduce frictional energy dissipation, which provides Coulomb damping.

Bearing stiffness depends on both the stiffness of the gas film and the stiffness of bump foil. In general, a bump-type foil bearing is designed so that the bump stiffness is much lower than the stiffness of the hydrodynamic gas film and therefore controls the overall stiffness of the bearing. This controlled stiffness leads to the desirable properties of being able to accommodate misalignment, tolerance variation, differential thermal expansion, and centrifugal shaft growth.

As a rule of thumb, the static load capacity of a foil bearing is determined by dividing the rotor weight (or preload for a vertical rotor) by bearing projected area. Typically, a design value of 1 to 5 psi is used. This small value helps minimize rubbing wear on the bearing surfaces during starts and stops. Through distributed film pressure, an external load applied to the bearing would be spread over several bumps. The load capacity is affected by two factors, namely, the maximum allowable bending stress of the bump foil and the ability to dissipate frictional heat generated on the bearing surfaces.

To replace the original tape-type bearing, the bore of the bearing housing was increased to accommodate the thicker bump foils and the fact that the bearing would be assembled in its own sleeve and then installed in the housing. Given the journal diameter of 0.63 in. and based on the availability of existing bump dies and foil material, several important dimensions were chosen:

- Diametric clearance = 0.002 in.
- Smooth foil thickness = 0.004 in.
- Bump foil thickness = 0.002 in.
- Bump height = 0.017 in.
- Bump pitch = 0.125 in.
- Bearing shell thickness = 0.1 in.

Therefore:

$$\text{Bearing shell ID} = 0.63 + 0.002 + 2x(0.002 + 0.004 + 0.017) = 0.678 \text{ in.}$$

$$\text{Bearing shell OD} \approx 0.88 \text{ in.}$$

As shown in Figure 9, these choices enabled three separate segments of bump foil (two with five bumps and one with four bumps), with space to weld them to the bearing shell. Since the compressor rotor is supported vertically, the bearing was preloaded radially for improved dynamic stability. To achieve this, a 0.0015-in. shim was installed at the middle of each bump segment.

ENGINEERING ANALYSIS METHODS FOR REPLACEMENT BEARINGS

Bump foil stress is a key parameter in the load-carrying capability of this type of bearing. In this application, we wanted a higher load capacity than the original tape-type bearing. Bump foil bearings are limited by their static load (rotor weight or preload) capacity, which is usually less than 5 psi (W/LD). This limit helps ensure easy start-up and minimizes surface wear of the top foil. At operating speeds when the gas film exists, the load capacity may increase by tenfold and ultimately be dictated by the tolerable bending stress in the bump foils. To survive in high-speed operation, the journal and foils must be cooled, which is usually done by channeling gas axially under the bump and around the shaft. Without adequate cooling, local thermal distortion may occur and quickly destroy the bearing. The other crucial parameter for successful high-speed operation is the amount of Coulomb damping in the bearing, which is required to prevent dangerous subsynchronous rotor whirl. Further details on the proper implementation of a bump bearing follow.

Bump Stress and Load Capacity

Figure 10 shows that under a compressive load, W , a typical foil bump moves downward by Δy and displaces horizontally at each end by Δx . The displacements are not only functions of the load, the elastic property of the foil metal, and the bump dimensions (radius of arc, foil thickness, foil pitch, etc.) but are also dependent on frictional coefficients at contact points. An existing two-dimensional (2-D) program HBUMSTR (Chen and Howarth, 2000) calculates the displacements and stiffness ($W/\Delta y$) with and without friction, given the foil dimensions and the remaining parameters and based on a uniformly distributed load.

Using this computer program and the desired static loading for the subject design ($W/pL = 1$ psi, p = bump pitch, L = bearing length), the bump foil calculation results are presented in Table 1. If the foil is made of Inconel, its heat-treated yield stress is about 150,000 psi. The table shows a bending stress of 4,200 psi based on the distributed load of 1 psi. Dividing the yield stress by the calculated bending stress, results in an allowable bearing load of 35.7 psi ($= 150/4.2$). The equivalent radial deflection is about 0.0035 in. ($= 35.7 \times 9.58 \times 10^{-5}$). These values compare favorably to the load limit and deflection of the original bearing (2.2 psi and 0.0014 in., respectively).

Heat Dissipation

Although its power loss is much smaller than a comparable oil-film bearing, a foil bearing does generate heat, principally by shearing levitating film. This heat can accumulate on the shaft and the top foil surface and cause their temperatures to rise. Because the foils are thin and contact areas are small, the heat conduction paths from top foil to bump foil and to the bearing housing are relatively poor. For most gas compressor applications, these are inadequate, and forced

convection heat transfer by injecting additional gas or liquid axially through the foils is required (Chen and Arora, 1986). For this cryogenic application, however, conduction plus natural convection proved adequate for removing the heat generated within the bearings.

An existing hydrodynamic journal foil bearing program HYJ (Chen and Howarth, 2000) calculates a number of bearing properties, including power loss, gas film pressure, bearing load, minimum film thickness, and so forth. This program treats the smooth foil as a bearing surface supported on a flexible foundation. Calculation results for the subject bearing are presented in Table 2, which shows a loss of 0.0052 hp with 1.17 lb loaded on a bearing of 0.63-in. diameter and 0.54-in. length at 90,000 rpm. This is a very small loss, which can be tolerated with no injected cooling gas. It should be noted, however, that the computer program does not consider the effect of preloads. The results therefore can only be taken as a reference.

Stiffness and Damping

Since fiction was not considered in the HYJ program, its stiffness output is not precise enough for rotordynamic analysis. Approximation by directly adding estimated Coulomb damping to the HYJ output stiffness is inappropriate. Peng and Carpino (1997) presented an elegant formulation for a foil bearing analysis, including a time-transient term in the Reynolds equation and foil-bump support with Coulomb damping, assuming that all the bumps can move circumferentially. To write a code based on this formulation would require a major effort, and to develop a code that considers all possible bump arrangements or configurations would be a complicated task to say the least. An issue was to determine if the top foil can be approximated without bending and membrane effects (Heshmat, et al., 1983; Carpino, et al., 1993). If so, the value of developing a complex and lengthy code as such is questionable. Although a rigorous computer code for generating foil bearing stiffness and damping properties may be ideal, it is not indispensable, considering the following:

- Many foil bearing parameters such as actual clearance and frictional coefficients are not well defined
- The gas film is in series with the bump foil but usually much stiffer than the bump foil. Ignoring the gas film, one may use the bump foil stiffness and damping properties to estimate the parameters of the rigid rotor modes, which may become unstable at high speed, and these are the main rotordynamic concern.
- The bump foil stiffness is not heavily dependent upon the friction coefficient, and may be estimated separately from the Coulomb damping.

As mentioned above, the bump foil stiffness can be calculated using the program HBUMSTR. Before presenting a method for estimating Coulomb damping, we shall discuss an optimal design for the bump foil configuration.

There are many variations in bump-type foil bearings. The top and/or bump foil can be one single piece or separated into several pieces. Furthermore, the bump foil can have different pitches or arc for varying radial stiffness in the circumferential direction. It can also have different layers for variable load capacity with varying eccentricity. Our experience indicates that a configuration such as that shown in Figure 9 typically works well. It has a one-piece smooth foil supported underneath by several bump foil sectors. Each sector is anchored at one end only, and four to six bumps ensure that the free end can slide circumferentially under radial load. This multiple sector design solves the low damping problem cited by Agrawal (1997).

Figure 11 presents a method that can be used to estimate the Coulomb damping in a bump foil. Considering a sector of five bumps is loaded evenly, each bump takes a radial load of W_1 lb. The bump top displaces by Δy in. and the bottom wants to displace by Δx in. in both directions. Since the sector is fixed at one end, the x displacements are accumulated as shown. Note that the free end has the most accumulated movement. Both the top and bottom of a bump have frictional contacts. The energy dissipated can be shown as:

$$E = 50\mu W_1 \Delta x$$

where μ = friction coefficient at the rubbing interfaces. Considering a vibration perturbation about the load, W_1 , an equivalent viscous damping coefficient would be:

$$B = 4E/\pi\omega\Delta y^2 \text{ lb-sec/in.}, \text{ then } \omega B = 4E/\pi\Delta y^2 \text{ lb/in.}$$

Using the data in Table 1, the foil bump stiffness for three preloaded segments was estimated to be $K = 5,040$ lb/in., and the equivalent viscous damping value for $\mu = 0.1$ was $\omega B = 5,800$ lb/in., assuming a radial vibration amplitude of 0.0005-in. peak. Since K and ωB have comparable values, there is therefore adequate Coulomb damping in the bearing.

Due to the fact that the vibration energy dissipation comes from rotor and foil bump displacements, it should be noted that there may always be small amounts of subsynchronous vibration in a frequency spectrum of a stably operating foil-bearing rotor.

FABRICATION OF REPLACEMENT BEARING

Figure 12 presents a typical fabrication, assembly, and inspection procedure (Grey, et al., 1981), with bearing parts in various stages of manufacturing shown in Figure 13. For the replacement bearing (Figure 14), the following rather straightforward steps were performed:

- Foil sheets of different thickness were made of Inconel X750 or similar material. The top smooth foil was cut into shape, and then heat treated in an argon gas environment in a furnace to a maximum temperature of about 1300°F to achieve desired hardness. The bearing side of the surface was then sprayed with an Emralon™ coating to provide a thin film of dry lubricant (DellaCorte, 2000). The foil was next rolled into cylindrical shape (see Figure 15) and attached to a stainless block at the fixed end. The spot welds at the block are at a larger radius than the smooth foil radius so that those welds would never contact the journal surface.
- For the bump foils, the Inconel sheets were cut to dimensions slightly larger than the finish sizes. These sheets were stacked together and cut to the final dimensions by wire EDM. Circumferential slits can be machined at the same time to enhance tolerance to axial misalignment. A 50-ton press and die were used to form the desired bumps in the sheets (see Figure 16). The bumped sheets were inserted into a cylindrical fixture (see Figure 17) with the proper diameter and heat treated in an argon gas environment to a maximum temperature of 1800°F for stress release and hardness (see Figure 18).
- The bump foils were spot welded into the bearing housing ID (see Figure 19). The top was then spot welded in place to finish the bearing assembly (see Figure 14).

- A two-step procedure for quality control was used. The first step involved a load versus deflection test on the assembled bearing, using only the small load required to move the journal through the bearing clearance. The second step involved a start-up liftoff test (see Figure 20) that was conducted by monitoring the bearing frictional torque versus shaft rotational speed. Bearing torque reduces significantly when the hydrodynamic film is established at a liftoff speed.

RESULTS OF COMPARISON TESTS

The compressor was operated with the original (tape-type) foil bearings to obtain baseline data for comparison to the replacement (bump-type) foil bearings. Vibration and bearing temperatures were also recorded. The replacement bearings were then installed and run.

Test Setup

Housing vibrations for the helium compressor were detected using accelerometers as shown in Figure 21 (Geren, et al., 2000). The unit was tested in open air with a dummy impeller. Resistance temperature detectors (RTD) were used to measure temperature at the bearing OD. In addition, thermocouples (not shown) were inserted near one end of the bump foil bearing to measure the nearby air flow temperature. Casing accelerations were taken at the impeller side in the x and y directions, at the other side in the x direction, and in the axial direction. Eddy-current-type displacement sensors were used to detect x and y displacements at the dummy wheel, but, unfortunately, both had large runouts. An eccentric rotor driven by a variable-speed motor was used as a shaker, which was mounted on one leg of the table supporting the compressor.

Liftoff and Touchdown Tests

When a foil bearing starts up from rest and accelerates to a speed high enough to form a hydrodynamic film, the frictional torque on the shaft reduces significantly. Associated changes include faster acceleration and reduced vibration. Touchdown during coastdown is marked by increased torque, faster deceleration, and increased vibration.

For the original bearings, shaft liftoff and touchdown were easy to determine. Visual observation of the tachometer showed a clear increase in acceleration when the rotor lifted off at approximately 23,000 rpm.

Due to its better operating characteristics, liftoff for the replacement bearing was not as obvious. Although there was no visual detectable change in speed, plotting the tachometer output versus time for speed-up and coastdown between 0 to 50,000 rpm allowed the determination that liftoff occurred in the 23,500-rpm range and touchdown occurred in the 15,000 to 19,000-rpm range (see Figure 22).

Steady-State and Transient Tests

For both types of bearings, the compressor was run at various speeds from 50,000 to 90,000 rpm for several hours. Steady-state vibration frequency spectra at 50,000 rpm are compared in Figure 23. Typical coastdown plots are presented in Figure 24. These plots reveal the following:

- A rotor critical speed was at 40,000 rpm with the original bearings; the corresponding critical speed with the replacement bearings was around 44,400 rpm. Based on the calculated critical speed map shown in Figure 7, these critical speeds were higher than expected. The thrust bearing may have contributed some dynamic angular stiffness. It is

also possible that the gas film at high speed tended to increase the foil load against the bearing housing. Frictional forces may have prevented the foil from moving freely in the circumferential direction, thus effectively making the bearing much stiffer.

- The replacement bearings had much lower casing vibration levels.
- The casing vibration spectra for the replacement bearing included a 2/rev signal, which could be indicative of loose parts or misalignment. However, the level was low and not considered a problem. At 90,000 rpm, the 2/rev component was significantly lower, as shown in Figure 25.

The original bearings were run with no cooling air and their temperature readings stabilized at about 120°F. As a precaution, the replacement bearings were initially run with 0.5-cfm cooling air, and temperatures stabilized at 100°F. Later runs showed that they can operate without cooling.

Shaker Tests

These tests were run to simulate the environment in which the compressor routinely operates. With the compressor running at 50,000 rpm, a dynamic shaker was used to excite the casing with a dynamic force of 0.01 g at 30 Hz. Typical responses are compared in Figure 26. The excited responses at 40,000 rpm confirm the critical speed located by coastdown tests. Further operational tests of the replacement bearings in the cryogenic environment are being proposed.

CONCLUSION

This paper has presented the engineering methodology involved in the design and fabrication of a bump-type radial foil bearing developed to replace a tape-type foil bearing in a helium turbocompressor. Future plans call for retrofit of an additional 25 machines with the bump-type bearing. In steady-state operation, test results showed that the replacement and original bearings operated in a similar manner. Both bearing types resulted in a critical speed around 40,000 rpm as confirmed by shaker tests. Since the critical speed is in the operating speed range, prolonged operation at this speed should be avoided. As this application example demonstrates, foil bearing technology is sufficiently mature for appropriate high-speed turbomachinery applications.

ACKNOWLEDGMENT

The authors gratefully acknowledge the contribution and guidance of Joel Fuerst at the Fermi National Accelerator Laboratory, the sponsor of this development effort and end user of the refit turbocompressors. At Foster-Miller Technologies, Peter Chapman, Robert Carr, and Terrance Bentley were key contributors to the design and fabrication of the replacement bearings, and at Turbotech Services, Mark Higgins, Len Ordon, and Ted DiMeo were the primary assembly and test operators. Richard Burchill, Vibration Consulting Services, Inc., recorded the test data and provided the associated analysis.

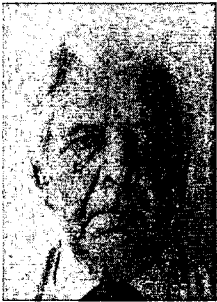
REFERENCES

- Agrawal, G. L. "Foil Air/Gas Bearing Technology - An Overview." Int'l Gas Turbine & Aeroengine Congress & Exhibition, Orlando, FL, June 2-5,1997, ASME 97-GT-347.
- Chen, S. H. and G. K. Arora. "Development of a 10,000 Start/Stop Cycle Foil Journal Bearing for a Gas Turbine Engine." AIAA/ASME/SAE/ASEE 22nd Joint Propulsion Conference, Huntsville, June 16-18,1986.
- Chen, H. M. and R. Howarth. *FMT Manual for Foil Bearing Computer Programs*. March 2000.
- DellaCorte, C. et al. *Performance and Durability of High Temperature Foil Air Bearings for Oil-Free Turbomachinery*. NASA/TM-2000-209187/Rev1, ARL-TR-2202, 2000.
- Gray, S., et al. "Technology Progress on Compliant Foil Air Bearing Systems for Commercial Applications." 8th Int'l Gas Bearing Symposium, Leicester Polytechnic, BHRA Fluid Engineering, Cranfield, Bedford, England, Paper 6, 1981.
- Geren, B. F., et al. "Phase II Replacement Foil Bearings for Helium Turbo Compressor." Report prepared by Turbotechnology Service Corp. for Fermi National Accelerator Lab, 2000.
- Heshmat, H., et al. "Analysis of Gas-Lubricated Foil Journal Bearings." *ASME Journal of Lubrication Technology*, Vol. 105, 1983, pp. 647-655.
- Ku, C.-P. R., and H. Heshmat, "Compliant Foil Bearing Structural Stiffness Part II: Experimental Investigation," *ASME Journal of Tribology*, 115, ASME 92-Trib-6, 1993.
- Ku, C.-P. R. and H. Heshmat. "Structural Stiffness and Coulomb Damping in Compliant Foil Journal Bearings: Theoretical Considerations." STLE Annual Meeting, Calgary, Canada, May 17-20, 1997.
- Licht, L. et al. "Dynamic Characteristics of a High-Speed Rotor with Radial and Axial Foil Bearing Supports." *Journal of Lubrication Technology*, Vol.103, pp. 361-372, July 1981.
- Oh, K. P. and S. M. Rhode. "A Theoretical Investigation of the Multileaf Journal Bearing." *ASME Journal of Applied Mechanics*, June 1976, pp. 237-242.
- Carpino, M., et al. "Effect of Membrane Stresses in the Prediction of Foil Bearing Performance." *STLE 93-AM-2E-1*, 1993.
- Peng, J. -P. and M. Carpino. "Finite Element Approach to the Prediction of Foil Bearing Rotor Dynamic Coefficients." *ASME, Journal of Tribology*, Vol. 119, January 1997.
- San Andres, L. "Turbulent Flow Foil Bearings for Cryogenic Applications." *Journal of Tribology*, Vol. 117, January 1995, pp. 185-195.
- Soyars, W. M. and J. D. Fuerst. "Fermilab Cold Compressor Bearing Lifetime Improvements." *Advances in Cryogenic Engineering*, Vol. 45B, Kluwer Academic/Plenum Publishers, New York, 2000, p. 1447.
- Vance, J. M. and L. San Andres. "Analysis of Actively Controlled Coulomb Damping for Rotating Machinery." ASME Paper No. 99-GT-175 presented at IGTI/ASME Congress, Indianapolis, IN, June 1999.

AUTHOR PHOTOS



Ming Chen.jpg



Roy Howarth.jpg



Bernard Geren.jpg

List of Figure and Table Captions
Application of Foil Bearings to Helium Turbocompressor
Chen, et al.

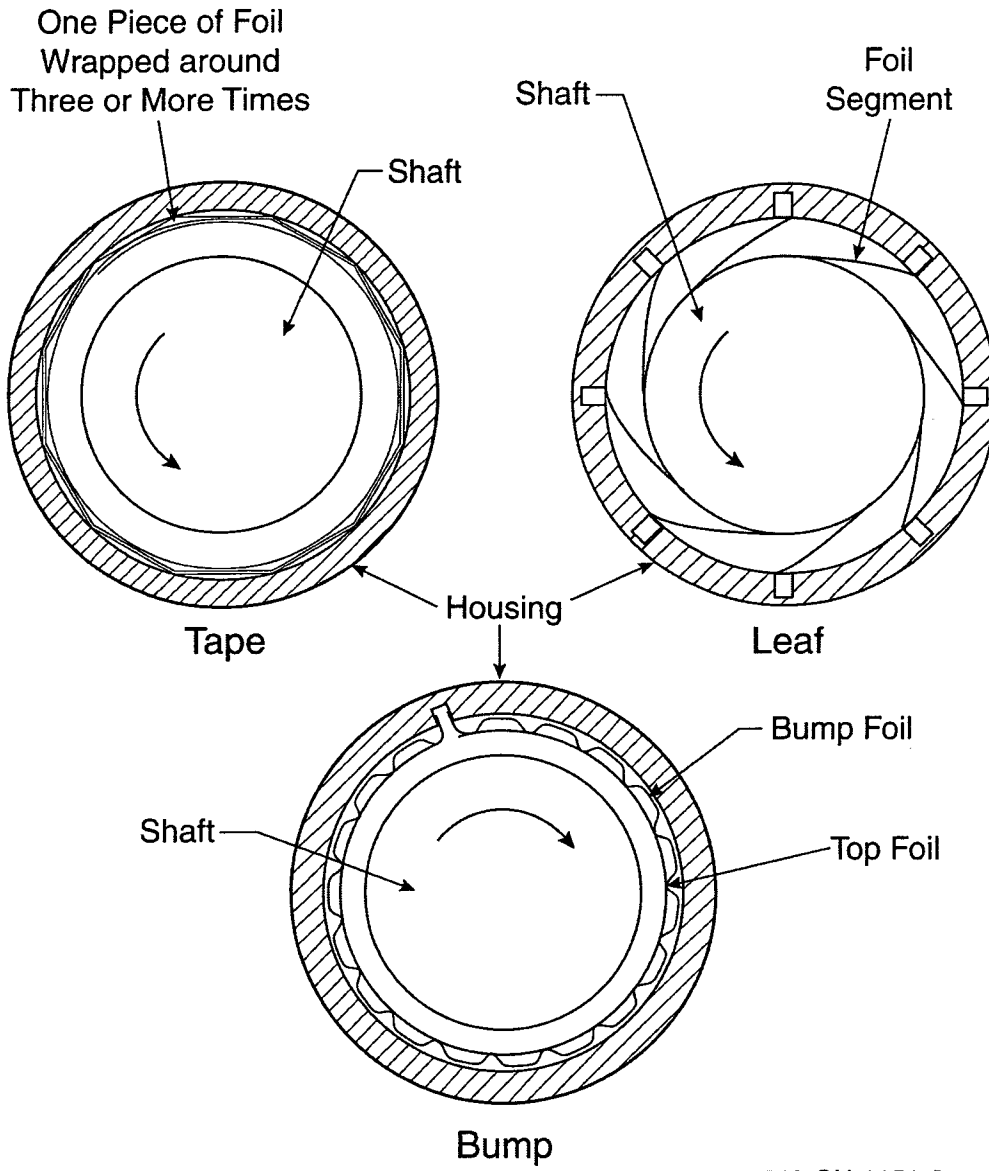
- Figure 1. Three Types of Foil Bearings
 - Figure 2. High-Speed Machinery Applications for Foil Bearings
 - Figure 3. Helium Turbocompressor (photo courtesy of Fermilab Visual Media Services)
 - Figure 4. Tape-Type Foil Bearing
 - Figure 5. Three Layers of Coils in Original (Tape Type) Bearing
 - Figure 6. Rotor Model
 - Figure 7. Critical Speed Map
 - Figure 8. Mode Shapes
 - Figure 9. Preloaded Bump Foil Bearing
 - Figure 10. Applied Load, Deflections, and Frictional Force of a Foil Bump
 - Figure 11. Estimation of Frictional Energy Dissipation of Foil Bumps
 - Figure 12. Foil Bearing Fabrication, Assembly, and Inspection Procedure
 - Figure 13. Bearings at Various Stages of Manufacturing Process
 - Figure 14. Replacement Bearing
 - Figure 15. Press used to Roll Foil into Shape
 - Figure 16. Foil Bump Die and Sample Bump Foil
 - Figure 17. Cylindrical Fixture used in Heat Treatment of Bumped Sheets
 - Figure 18. Heat Treatment of Bumped Sheets
 - Figure 19. Spot Welding of Bump Foils into Bearing Housing ID
 - Figure 20. Setup for Start-up Liftoff Test
 - Figure 21. Test Setup
 - Figure 22. Start-up and Coastdown Speed Acceleration Amplitudes versus Time
showing Lift-off and Touchdown Speeds
 - Figure 23. Steady-State Vibration Frequency Spectra at 50,000 rpm
 - Figure 24. Typical Coastdown Plots
 - Figure 25. Steady-State Vibration Frequency Spectra at 90,000 rpm for Replacement
Bearing
 - Figure 26. Typical Bearing Response during Shaker Tests
-
- Table 1. Calculated Properties of Bump Foil from HBUMSTR Program
 - Table 2. Calculated Properties of Gas Film from HYJ Program

Table 1. Calculated Properties of Bump Foil
from HBUMSTR Program

Input	
0.002	Bump thickness, in.
0.093	Bump length, in.
0.017	Bump height, in.
0.125	Bump pitch, in.
0.004	Tape thickness, in.
0.1	Friction coefficient
Output	
7.21E-02	Bump radius, in.
8.033E+01	Subtended angle, deg
9.577E-05	Deflection, in.
1.305E-03	Stiffness, psi
-3.125E+00	Central stress, psi
4.200E+03	Bending stress, psi
1.196E-05	Lateral deflection, in.
3.725E-06	Upper tape deflection, in.
1.244E+03	Stiffness at 0 friction, psi

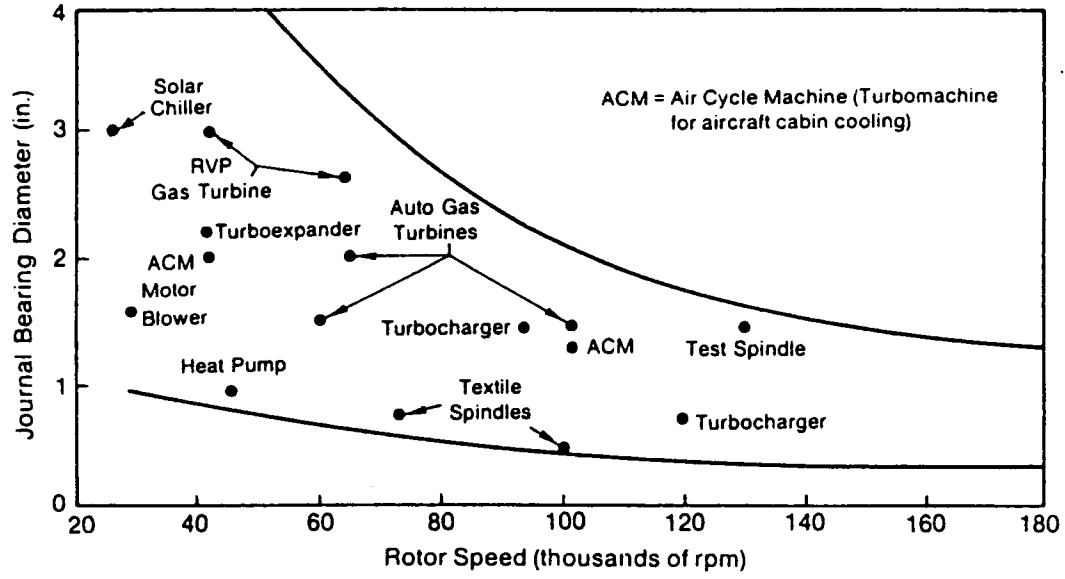
Table 2. Calculated Properties of Gas Film
from HYJ Program

Input	
199	Angle CCW from y-axis to eccentricity, deg
355	Angle CCW from TH1S to beginning of taper, deg
0.547	Bearing length, radius
0.315	Bearing radius, in.
90000	Rotational speed, rpm
11	Mesh lines along axial direction
51	Mesh lines along circumferential direction
2.93e-9	Lubricant viscosity, lb-sec/in.**2
1.0e-3	Radial clearance, in.
1309	Bump foil stiffness, psi
14.7	Ambient pressure, psig
0.125	Bump pitch, in.
0.95	Eccentricity ratio
2	TH1S Start of pad, deg
357	TH1E End of pad, deg
Output	
-1.784E-04	Horizontal component of load, lb
1.169	Vertical component of load, lb
1.169	Load capacity, lb
-8.740E-03	Load angle, deg, CW from y-axis
5.203E-03	Power loss, hp
0.559	Nominal min. film thickness, mil
5.543	Maximum pressure, psig
1427	Kxx, lb/in.
-579	Kyx, lb/in.
-69	Kxy, lb/in.
1654	Kyy, lb/in.



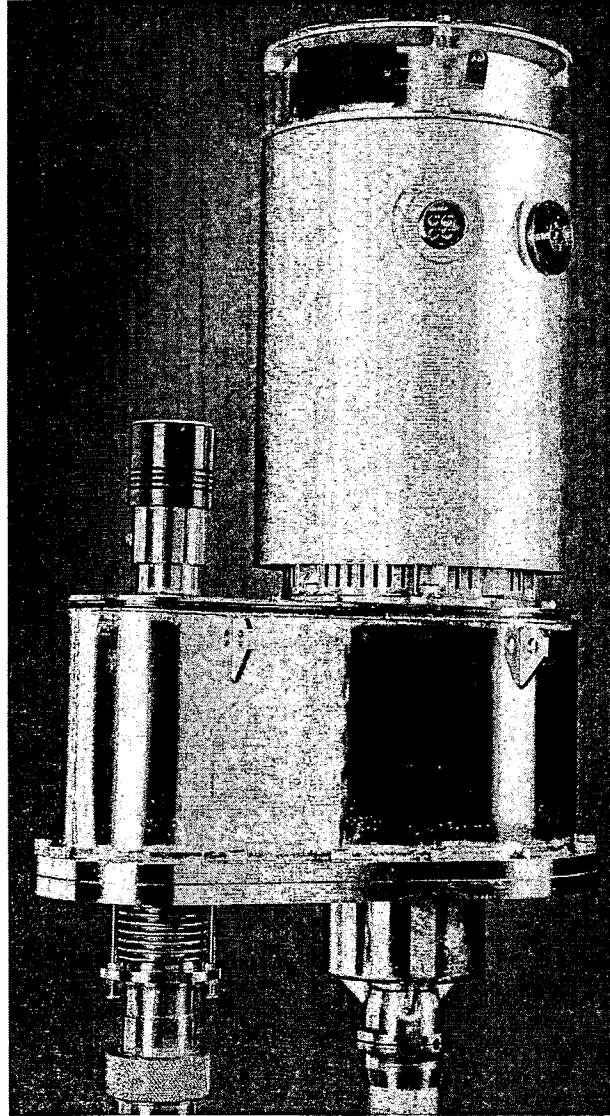
549-OH-1151-2

Figure 1. Three Types of Foil Bearings



00010

Figure 2. High-Speed Machinery Applications for Foil Bearings



01ph22

Figure 3. Helium Turbocompressor
(photo courtesy of Fermilab Visual Media Services)

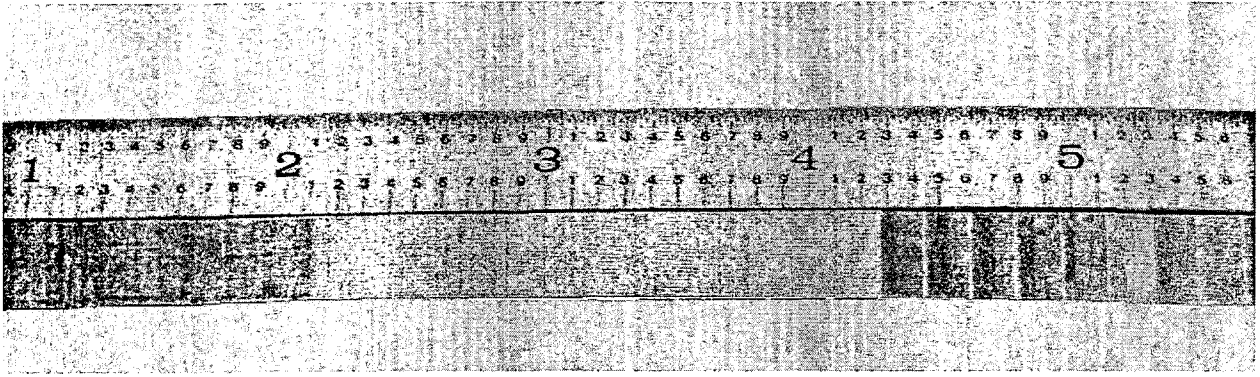
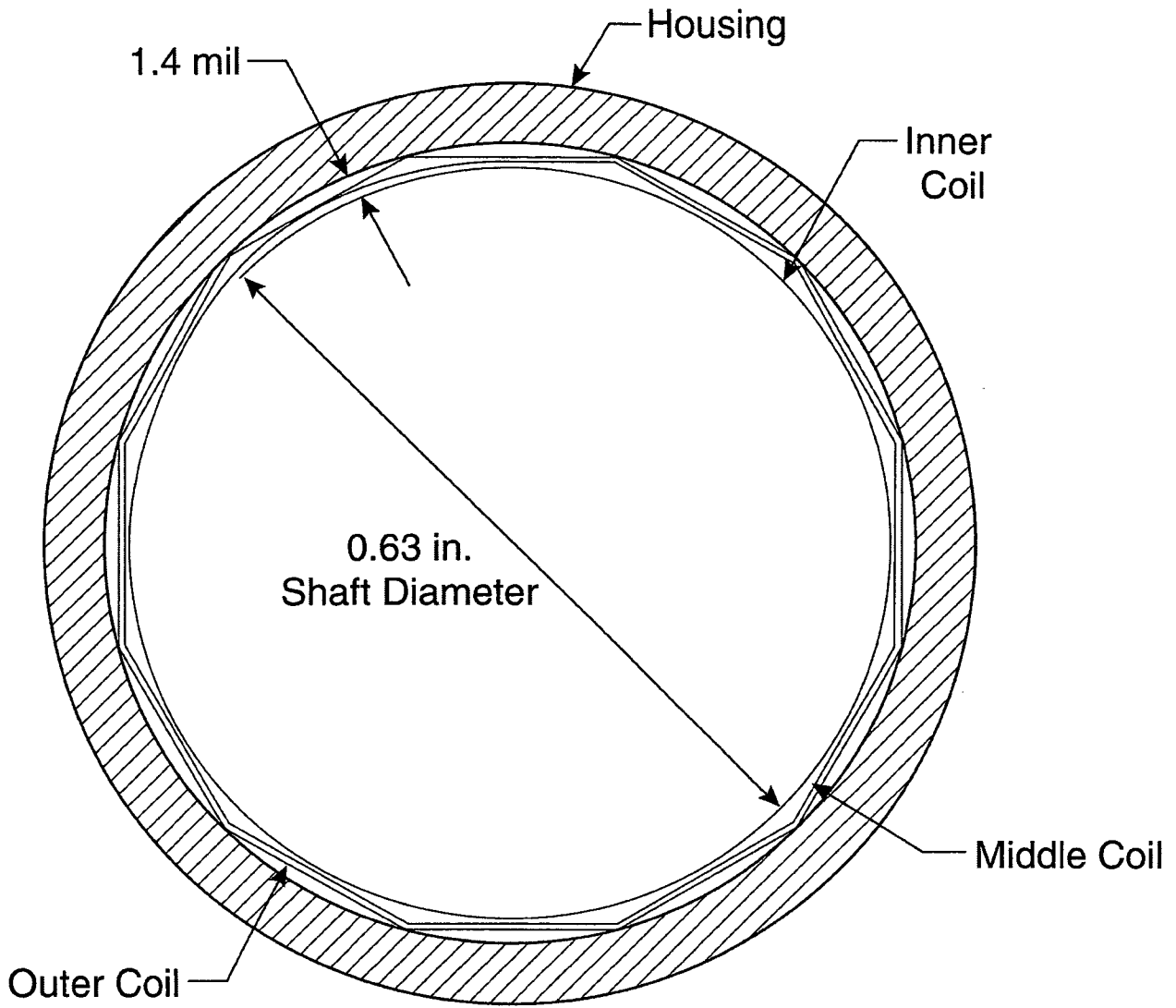


Figure 4. Tape-Type Foil Bearing



549-OH-1151-1

Figure 5. Three Layers of Coils in Original (Tape Type) Bearing

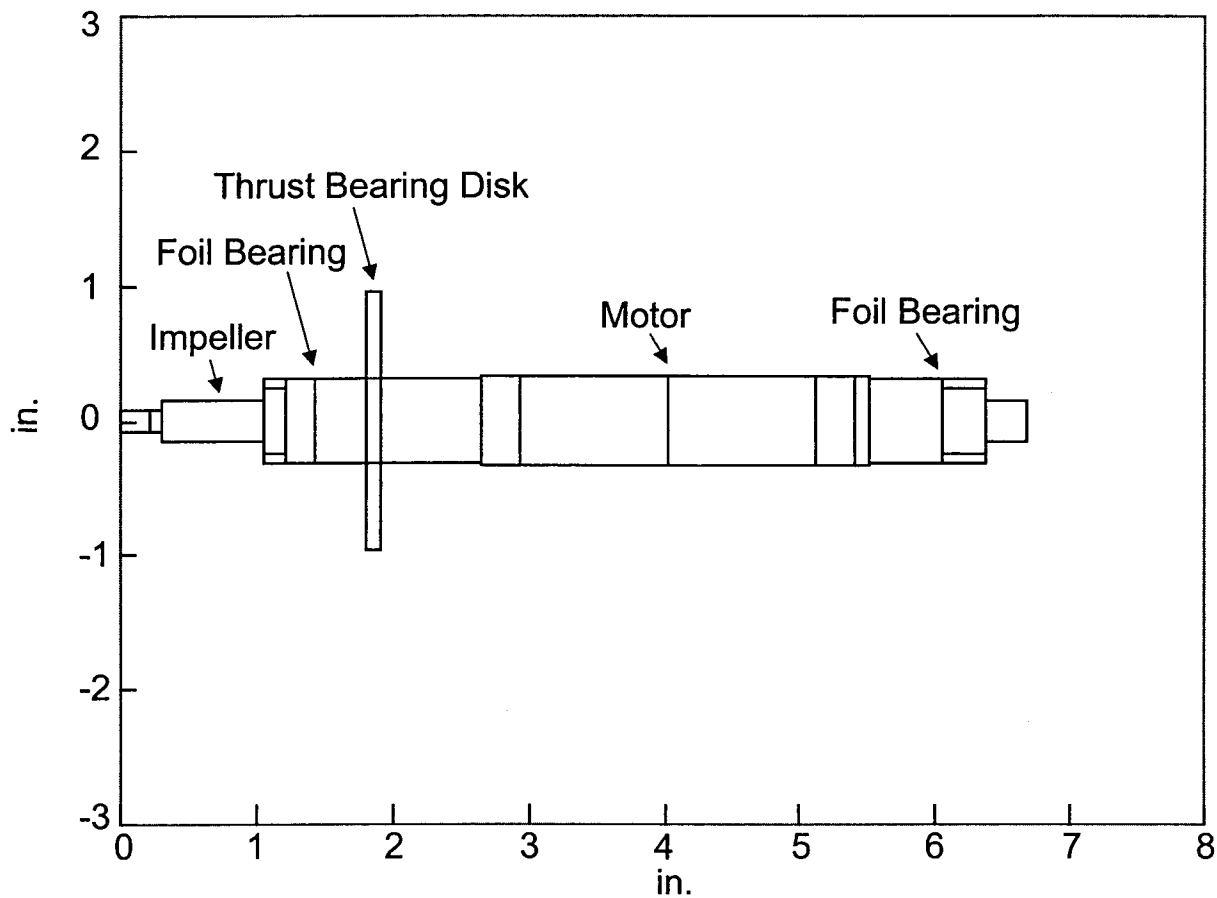


Figure 6. Rotor Model

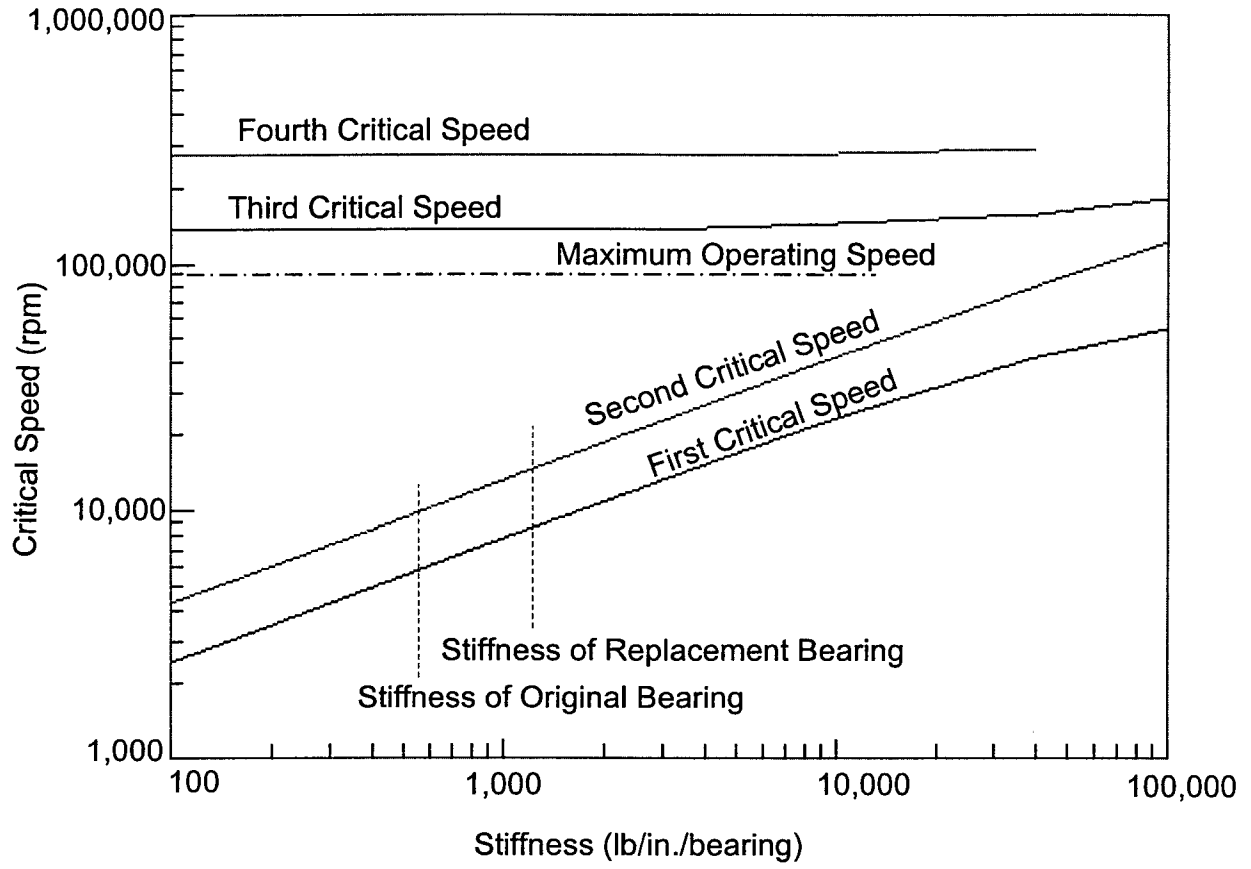


Figure 7. Critical Speed Map

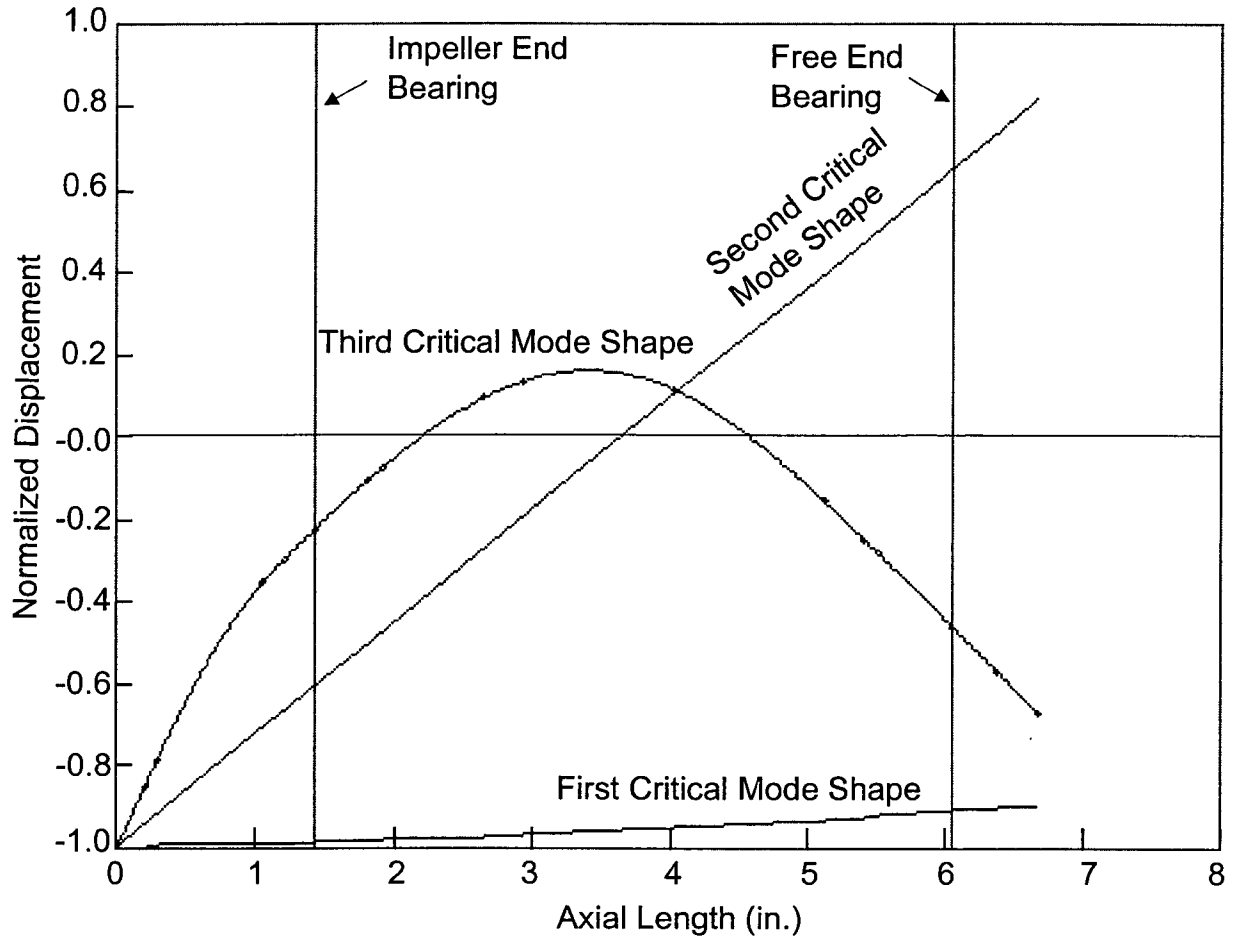


Figure 8. Mode Shapes

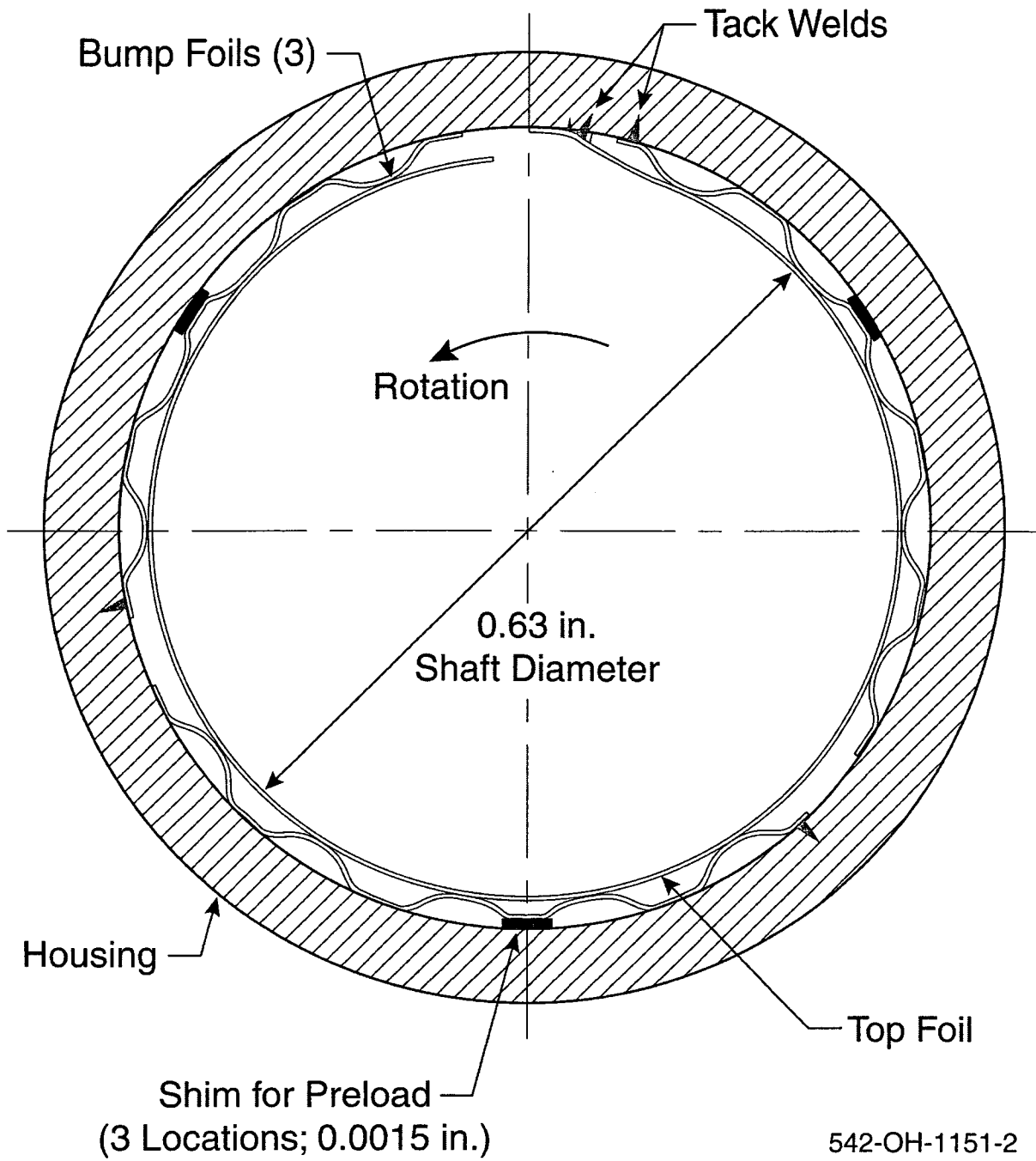


Figure 9. Preloaded Bump Foil Bearing

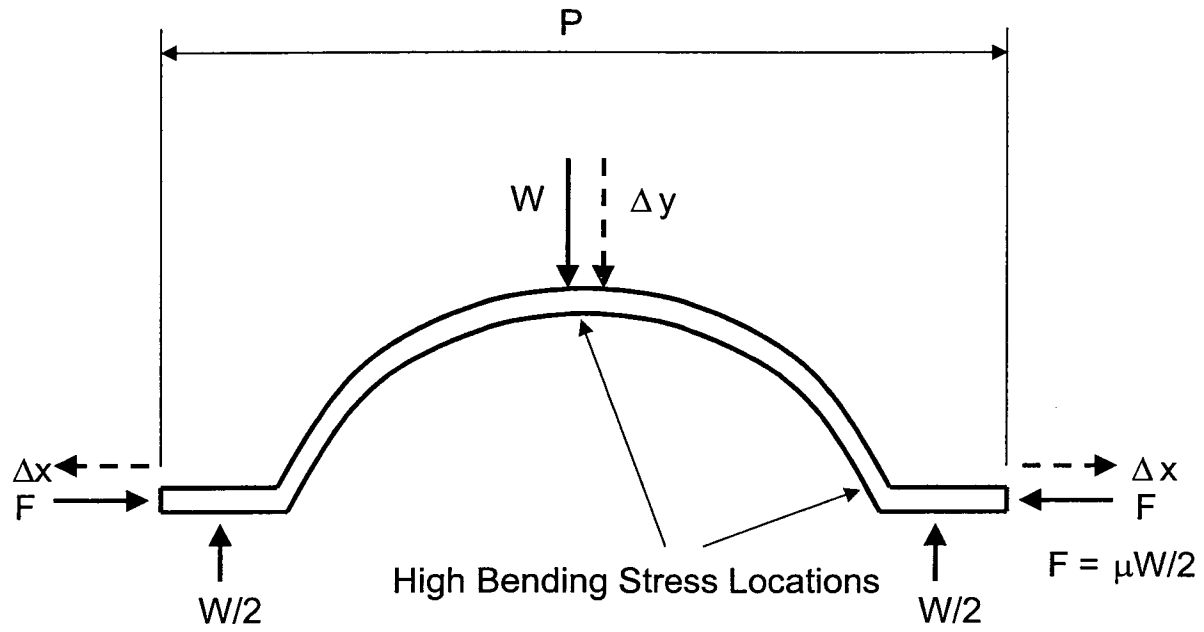


Figure 10. Applied Load, Deflections, and Frictional Force of a Foil Bump

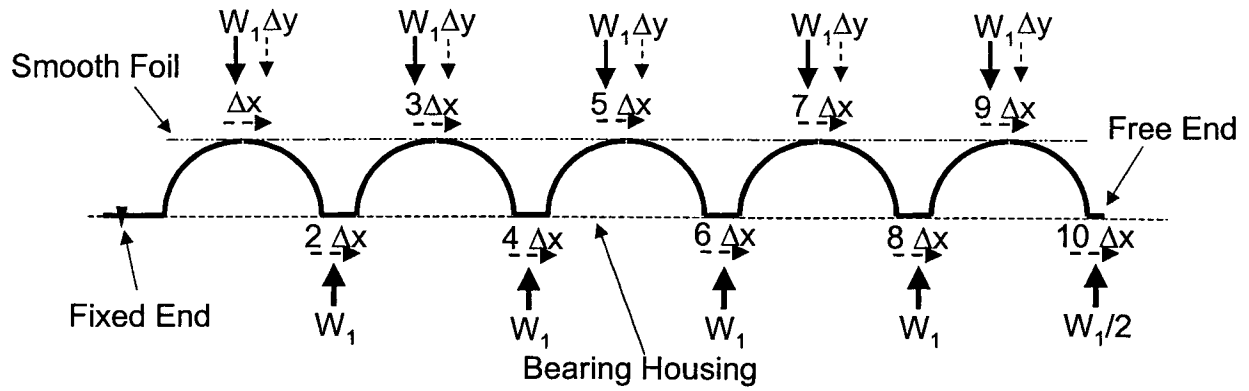
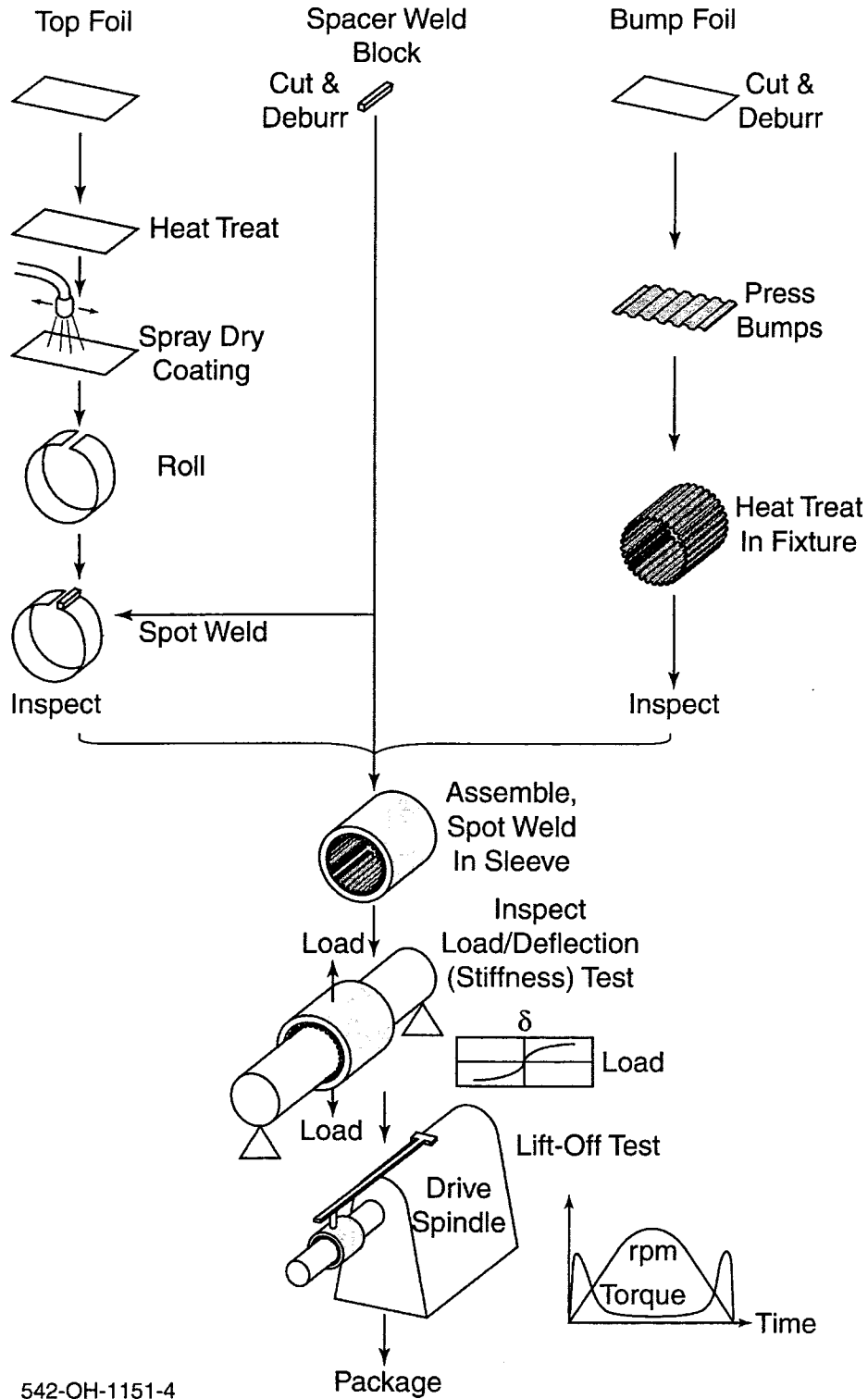


Figure 11. Estimation of Frictional Energy Dissipation of Foil Bumps



542-OH-1151-4

Figure 12. Foil Bearing Fabrication, Assembly, and Inspection Procedure

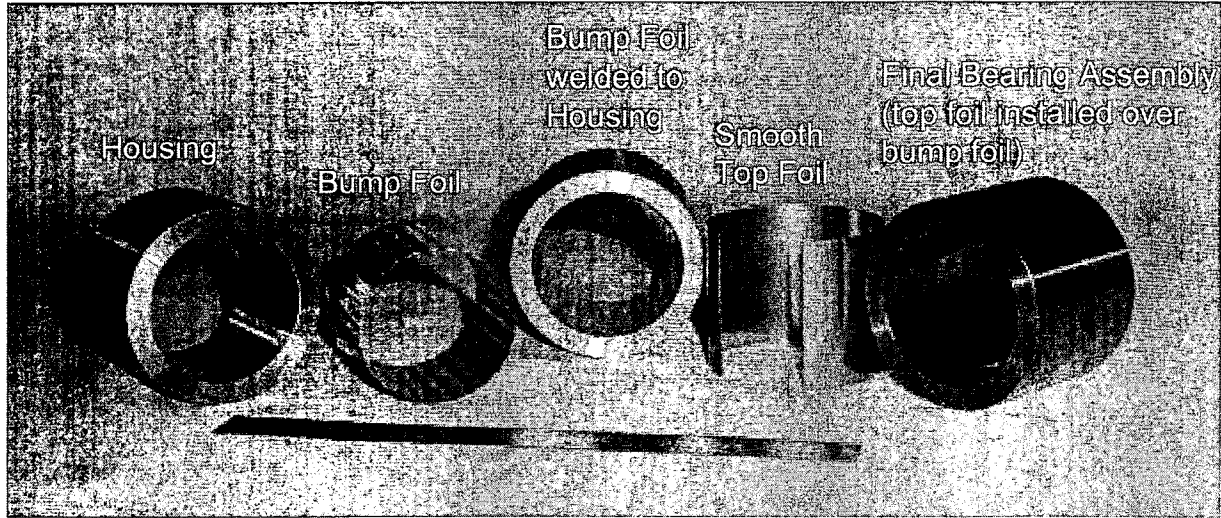


Figure 13. Bearings at Various Stages of Manufacturing Process

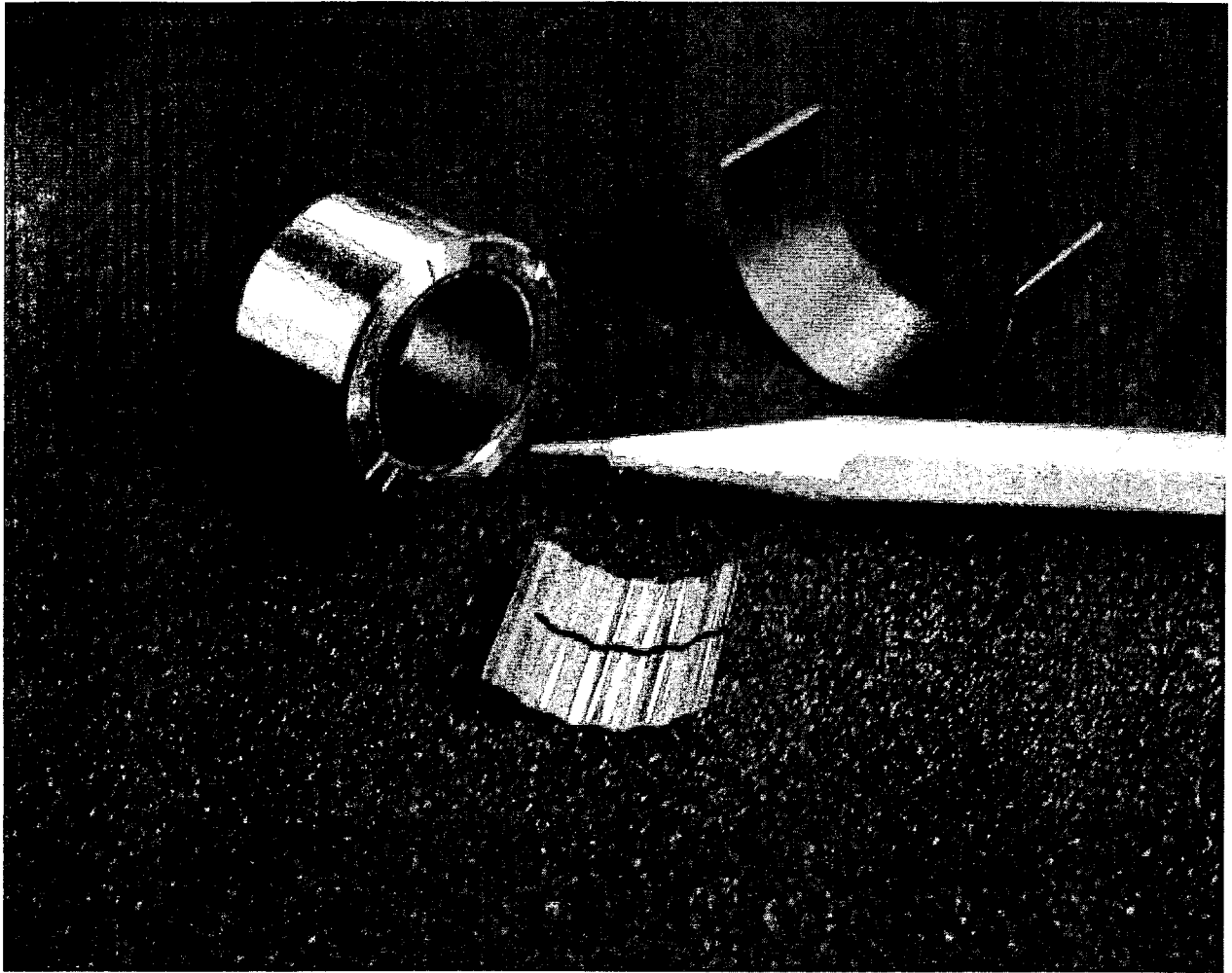


Figure 14. Replacement Bearing

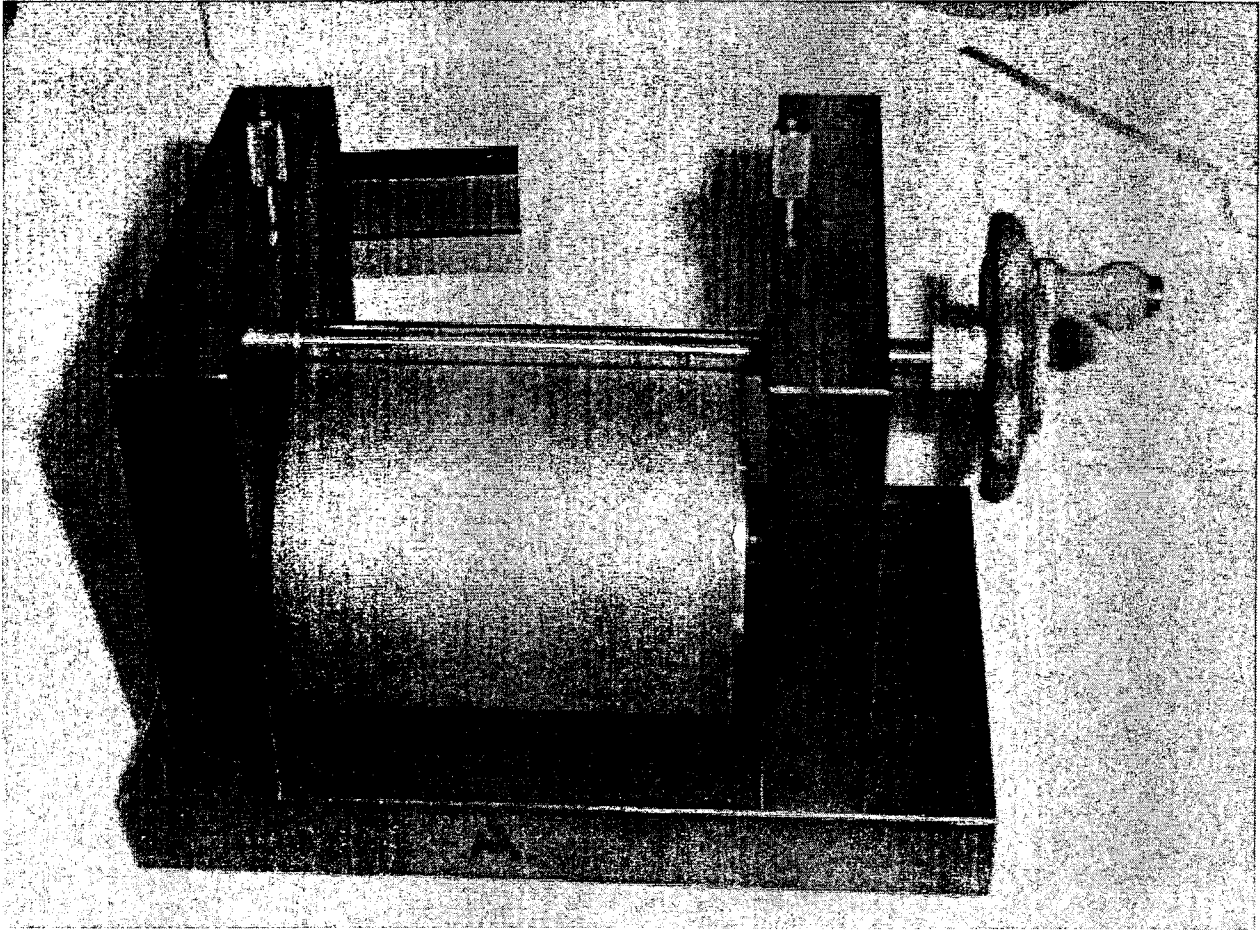


Figure 15. Press used to Roll Foil into Shape

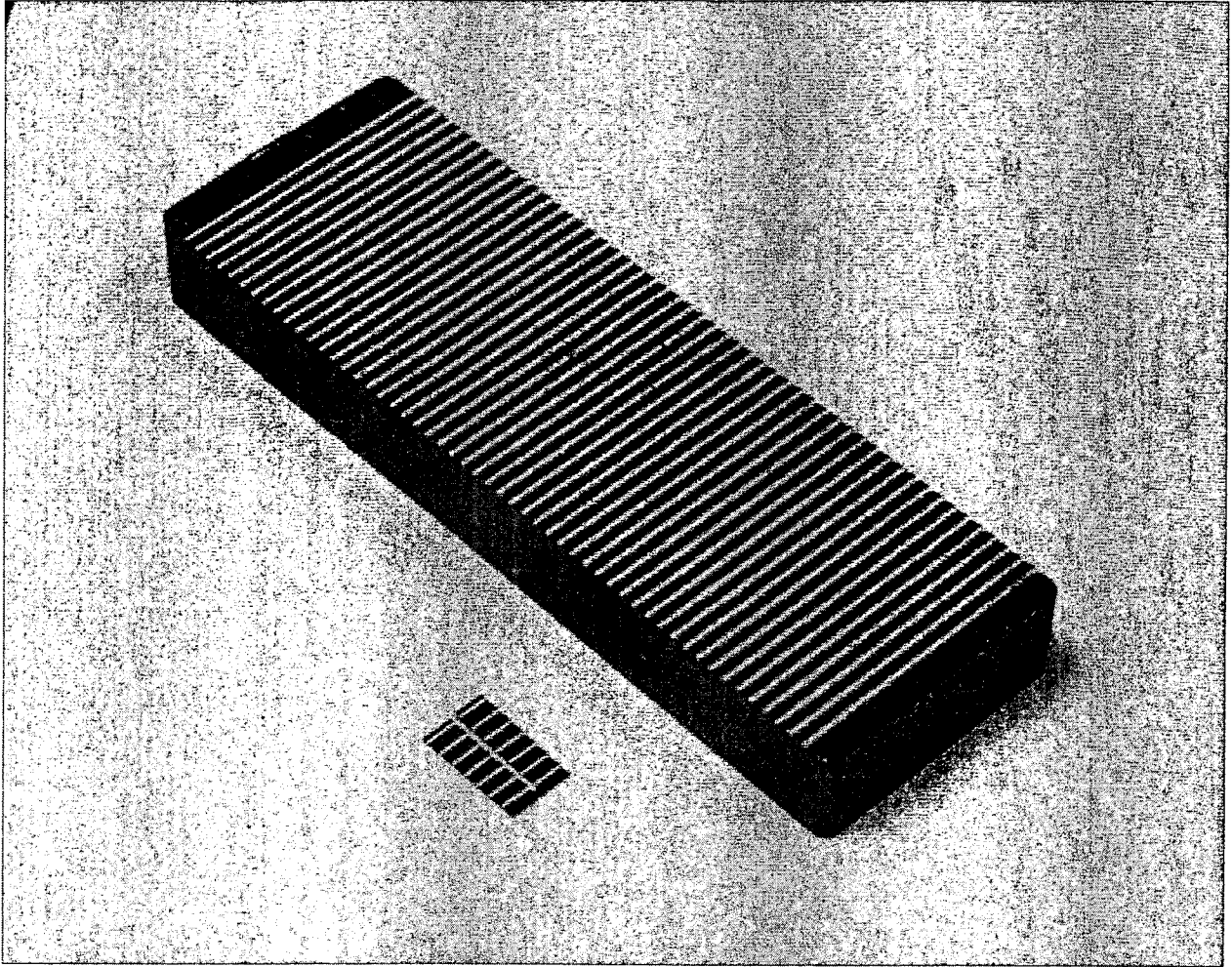


Figure 16. Foil Bump Die and Sample Bump Foil

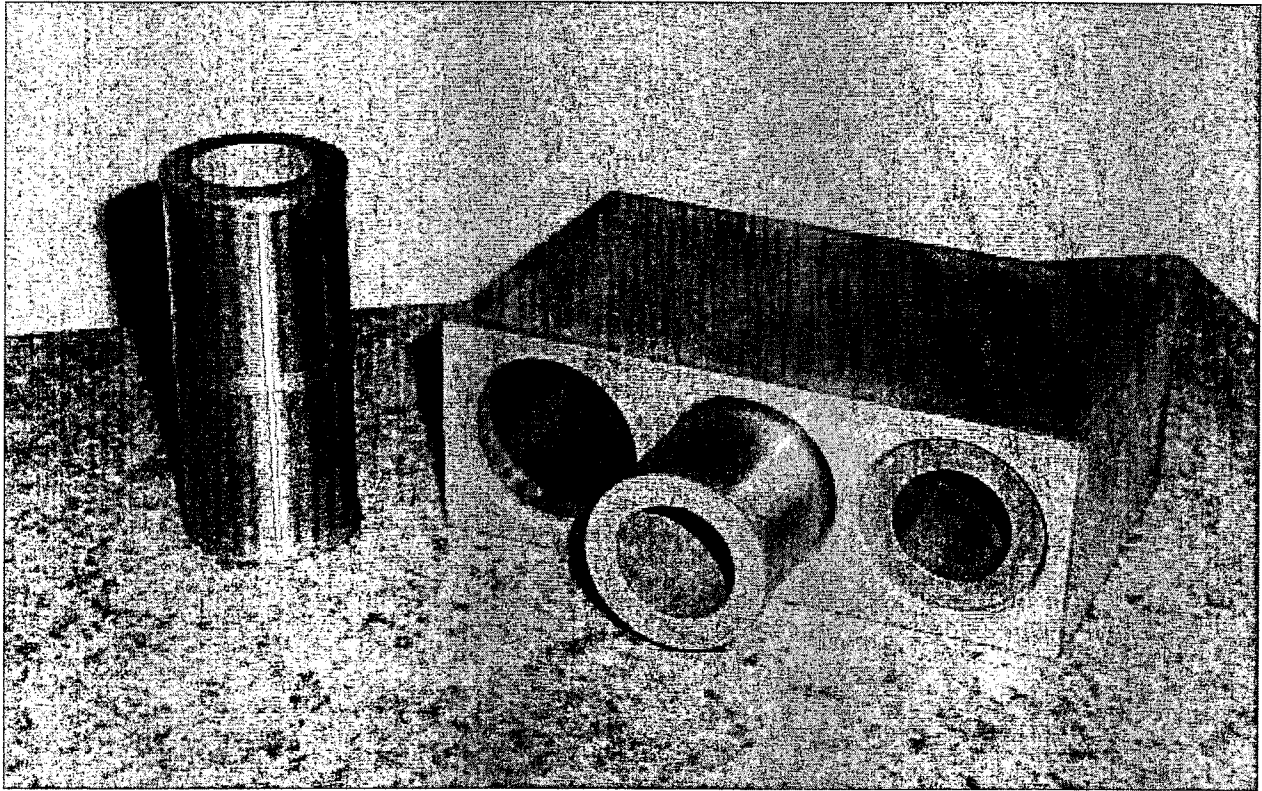


Figure 17. Cylindrical Fixture used in Heat Treatment of Bumped Sheets

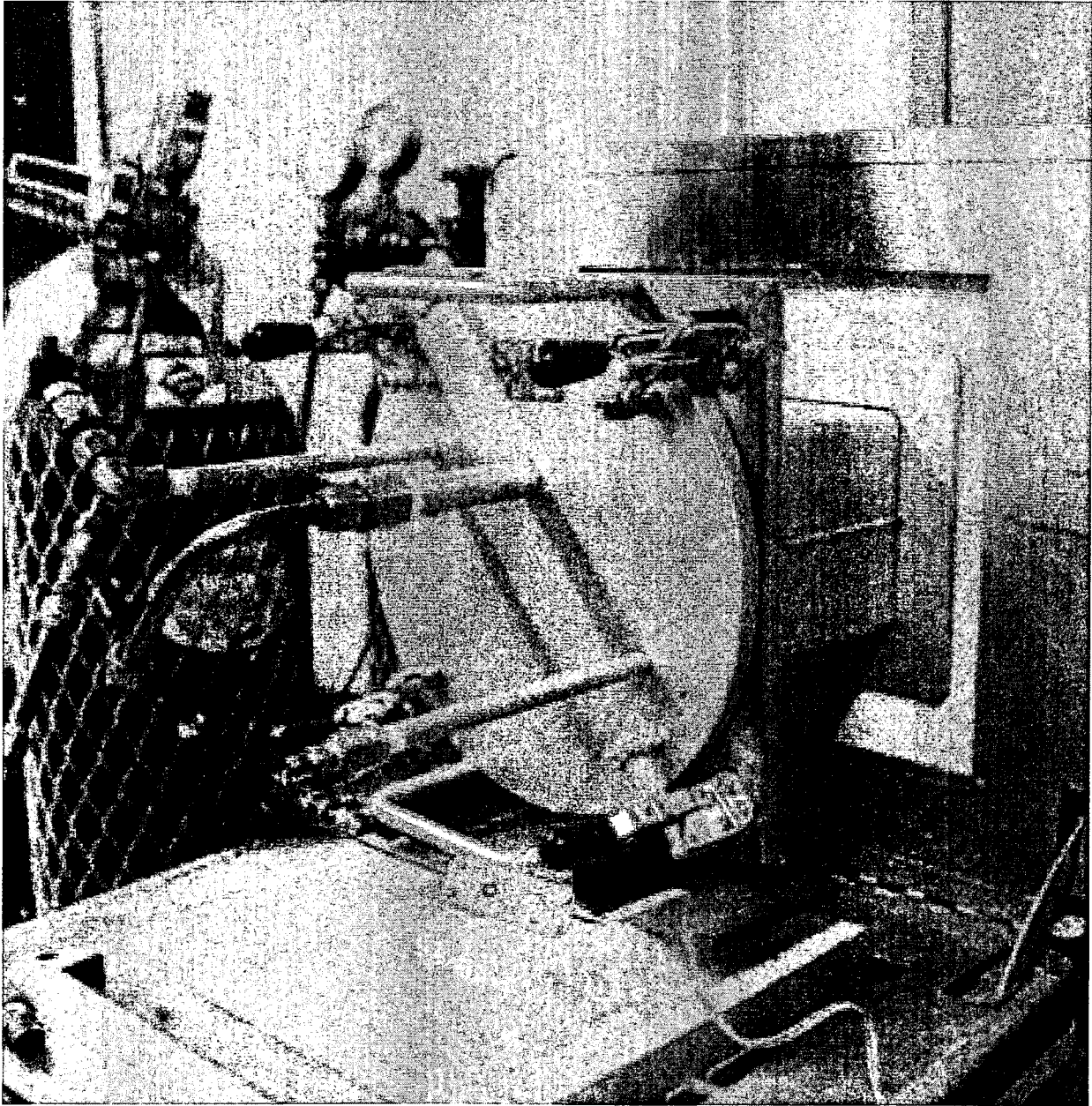


Figure 18. Heat Treatment of Bumped Sheets

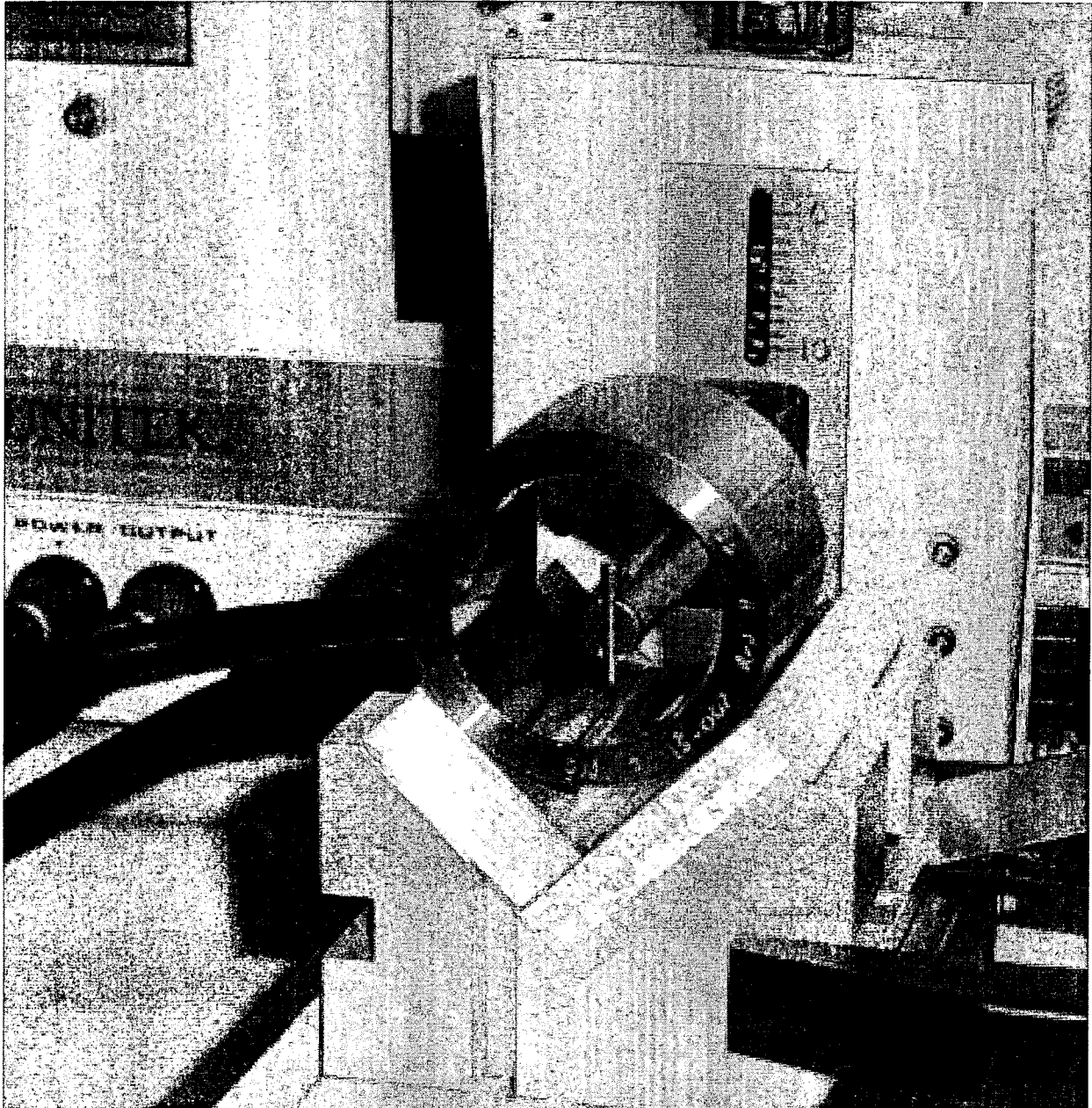


Figure 19. Spot Welding of Bump Foils into Bearing Housing ID

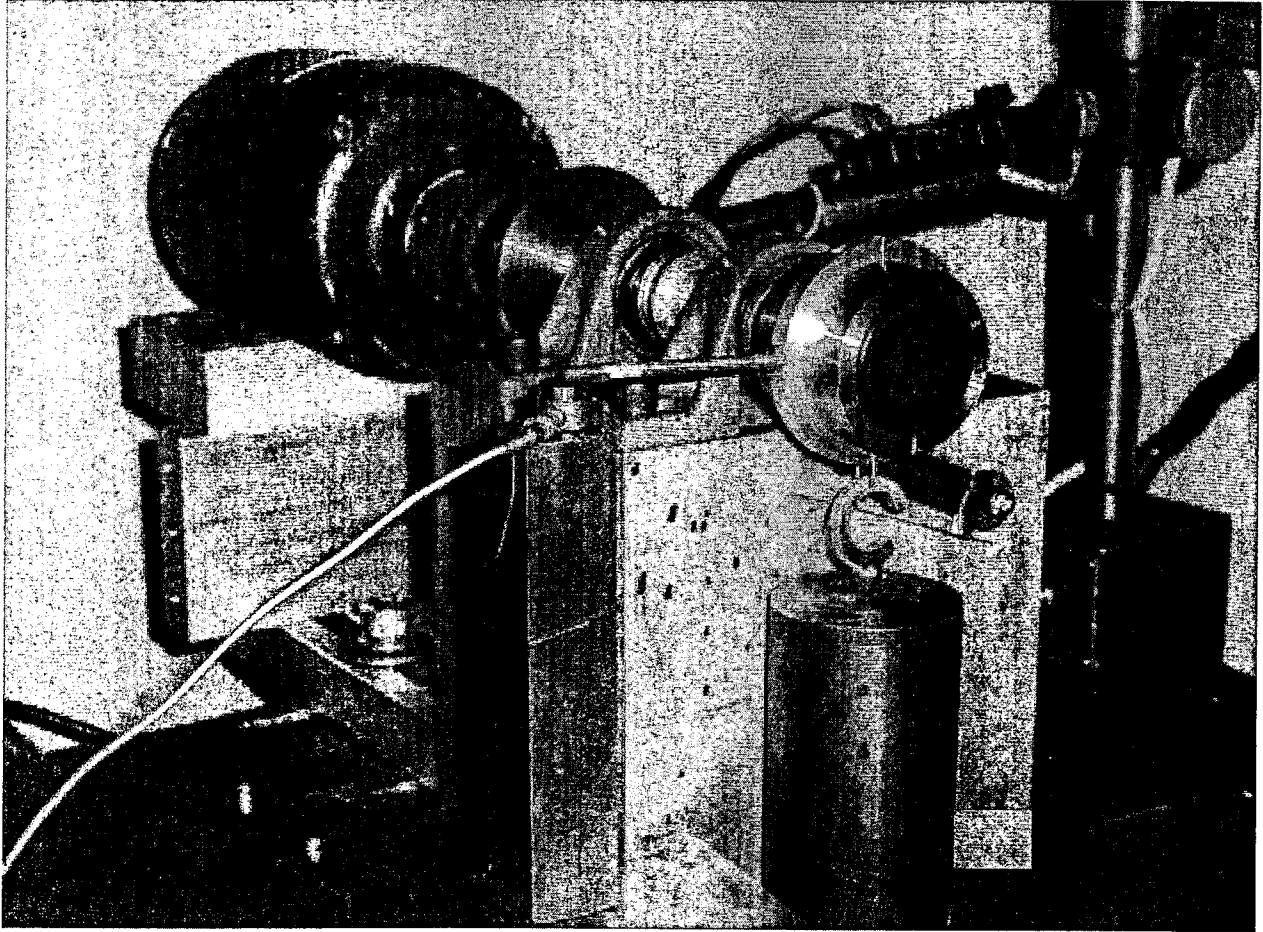


Figure 20. Setup for Start-up Liftoff Test

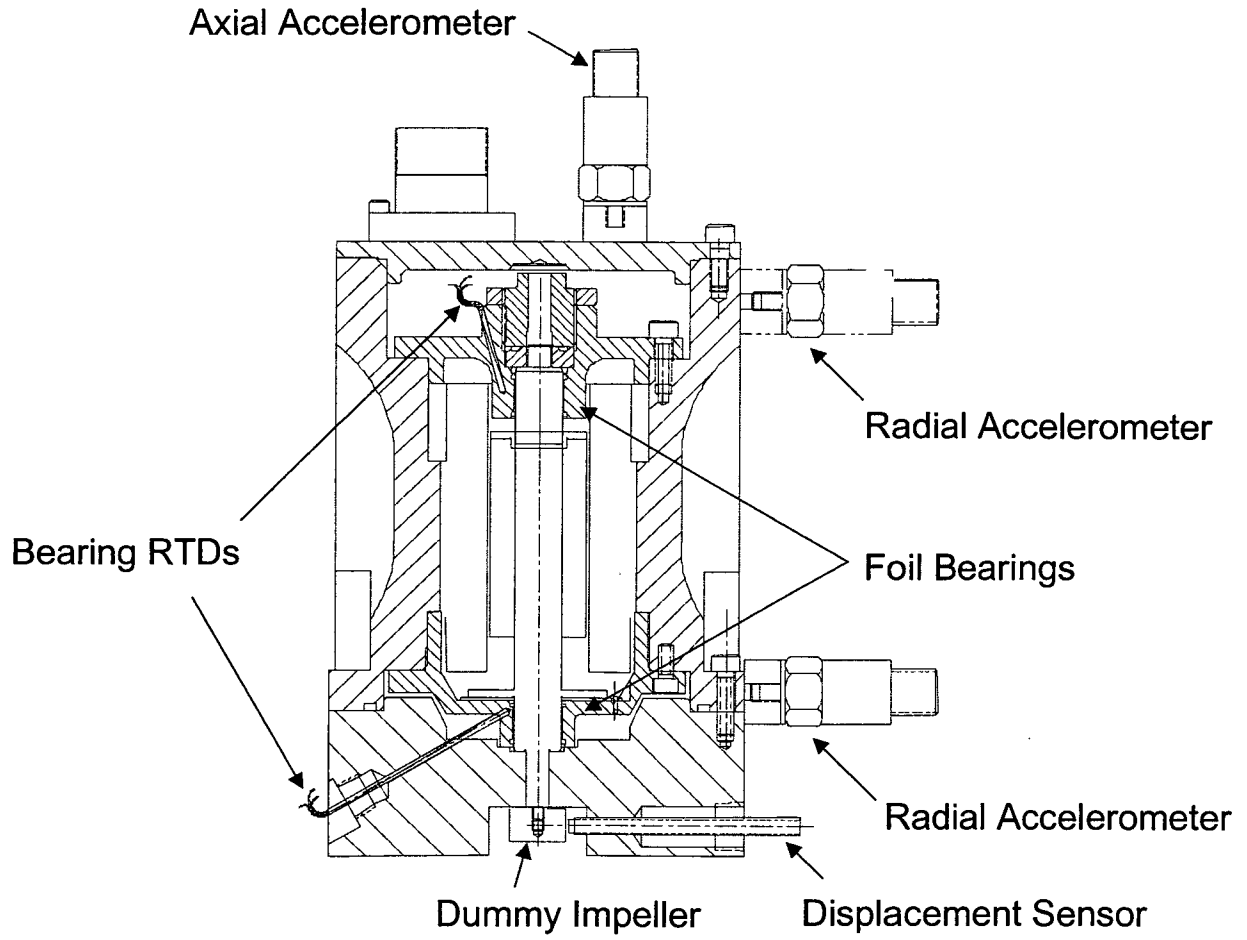


Figure 21. Test Setup

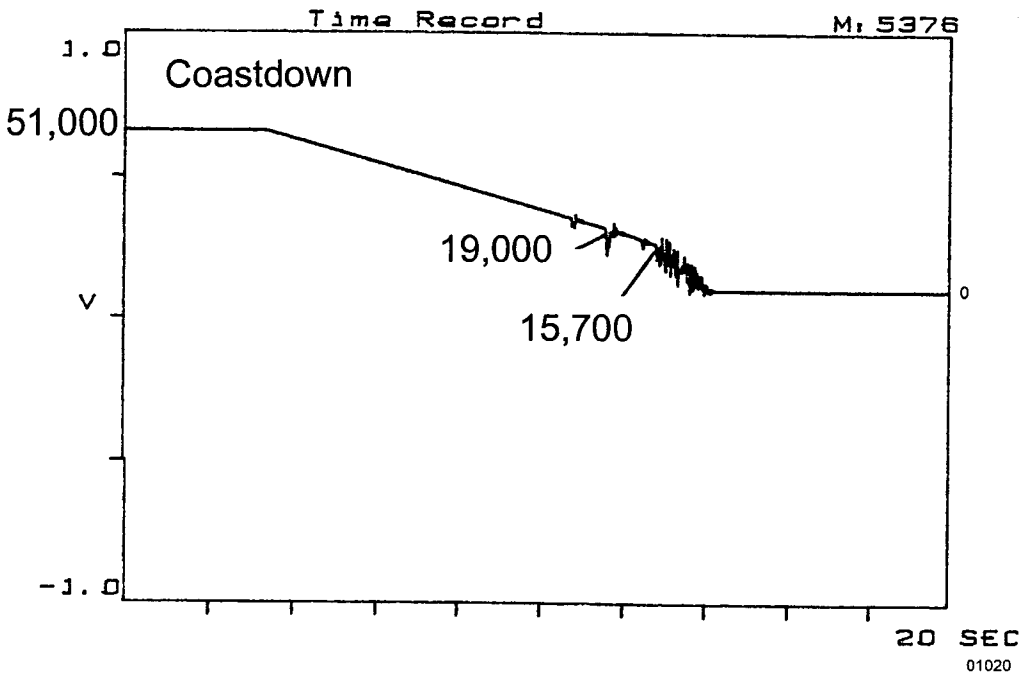
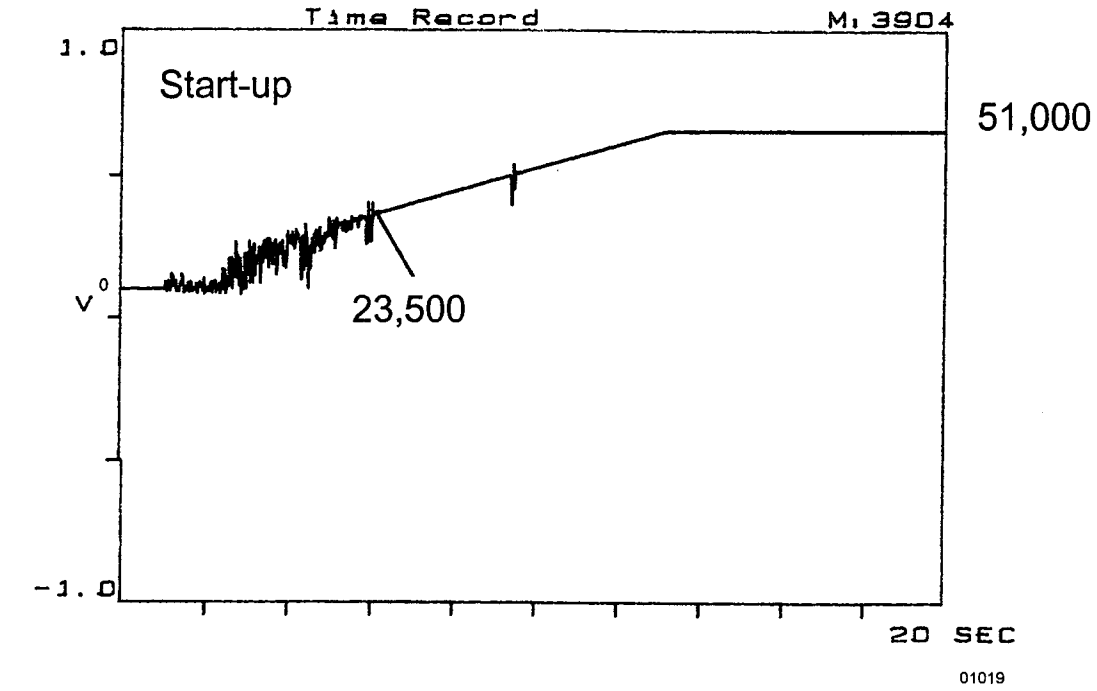


Figure 22. Start-Up and Coastdown Speed Acceleration Amplitudes versus Time Showing Lift-Off and Touchdown Speeds

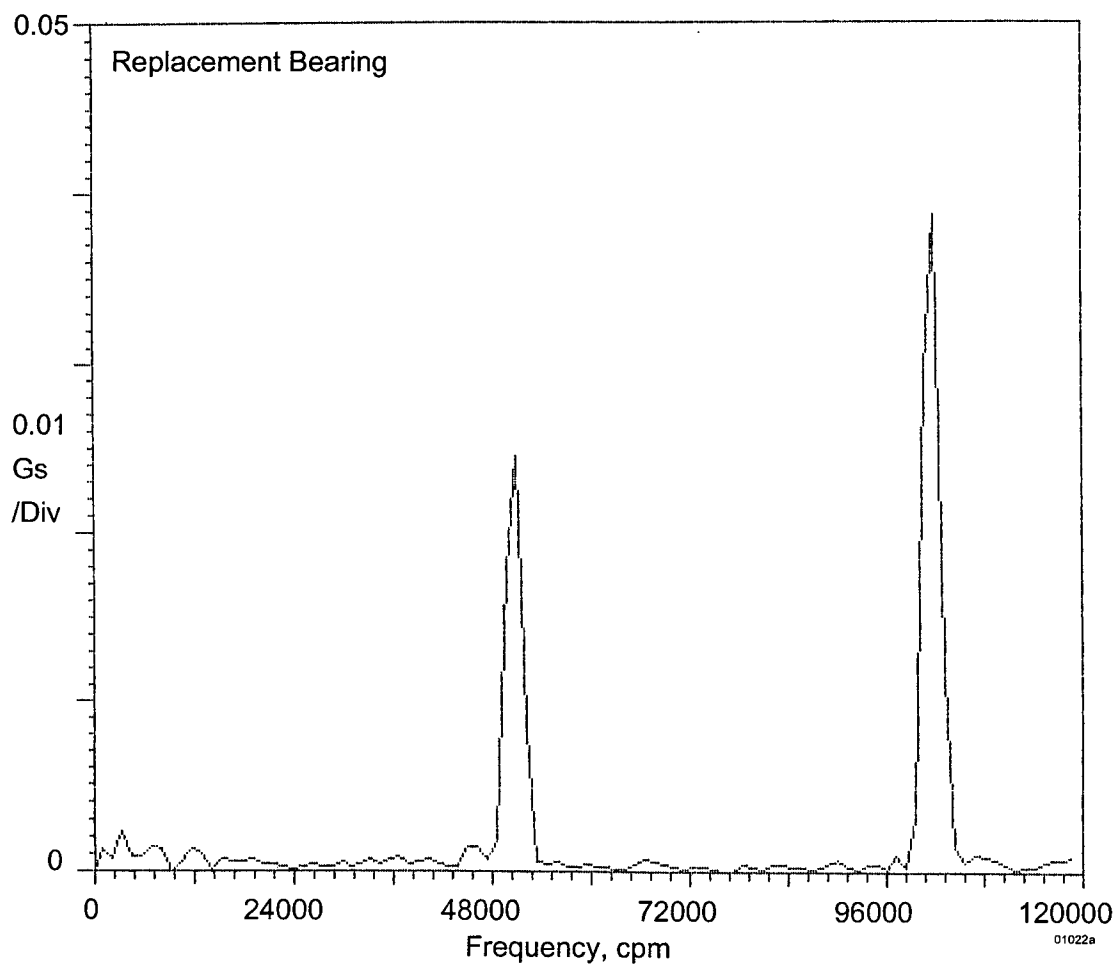
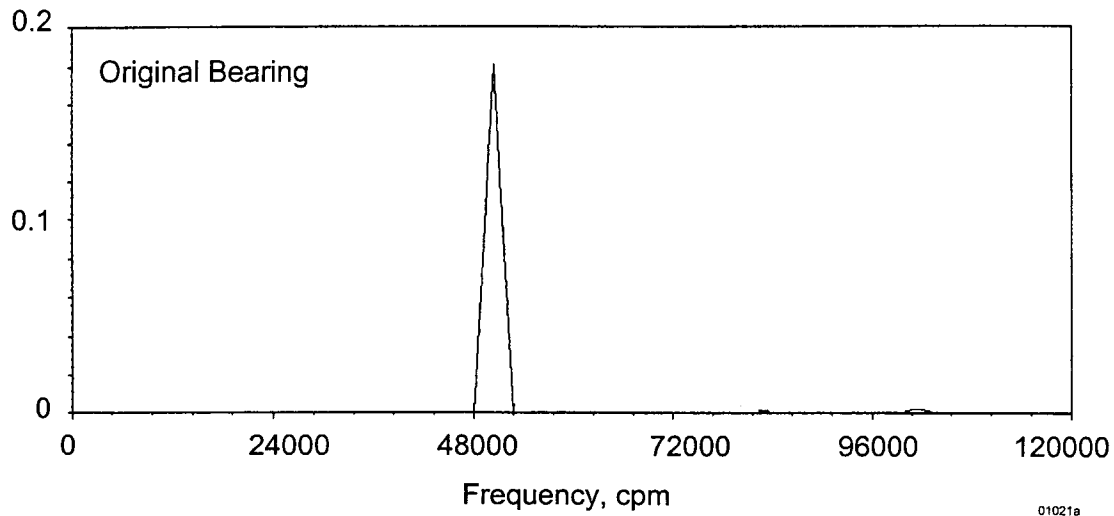


Figure 23. Steady-State Vibration Frequency Spectra at 50,000 rpm

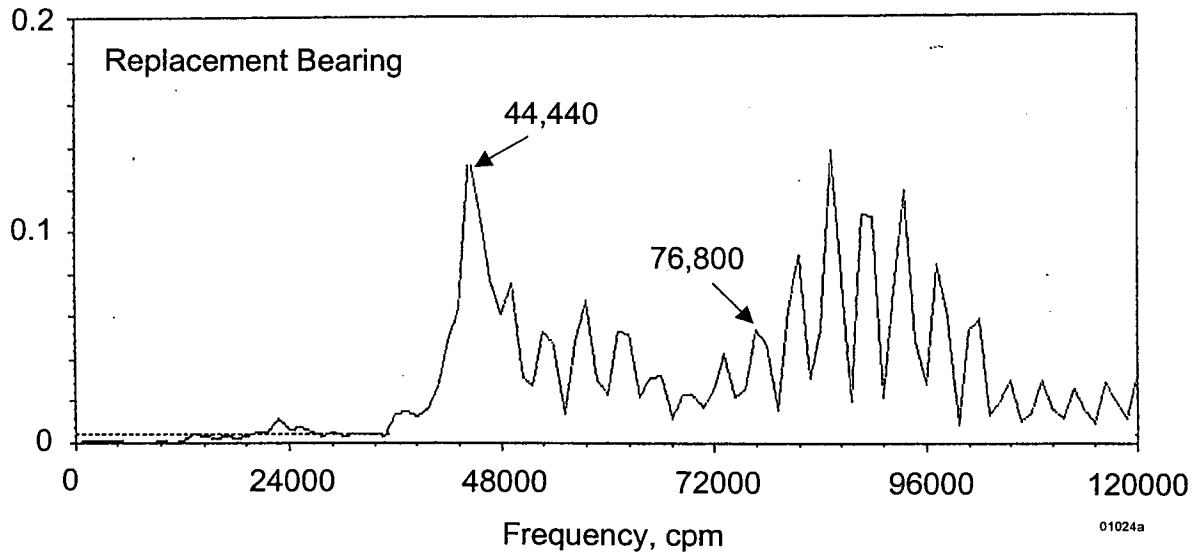
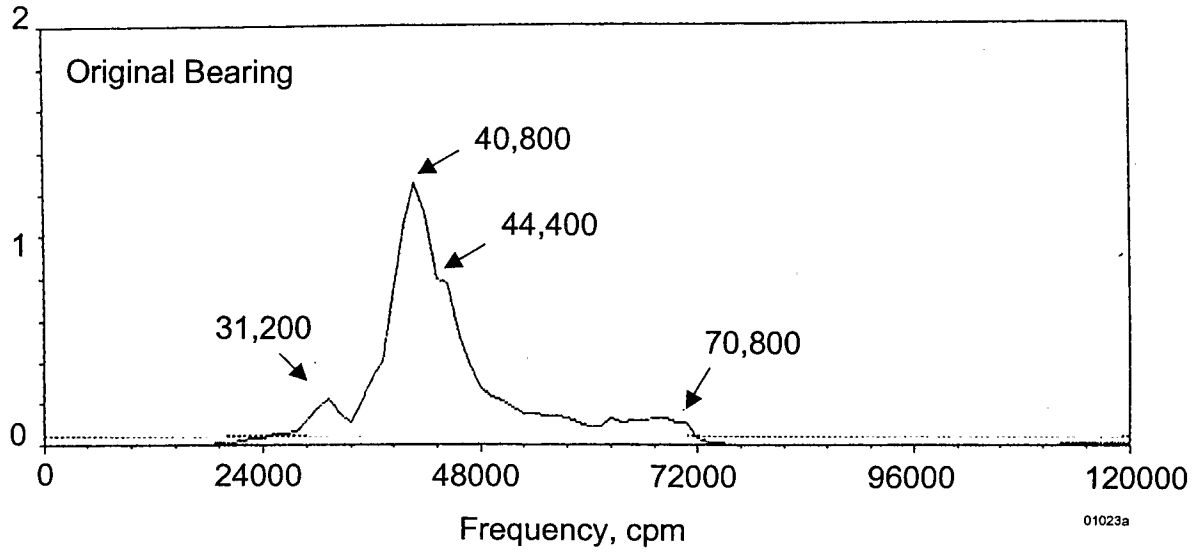


Figure 24. Typical Coastdown Plots

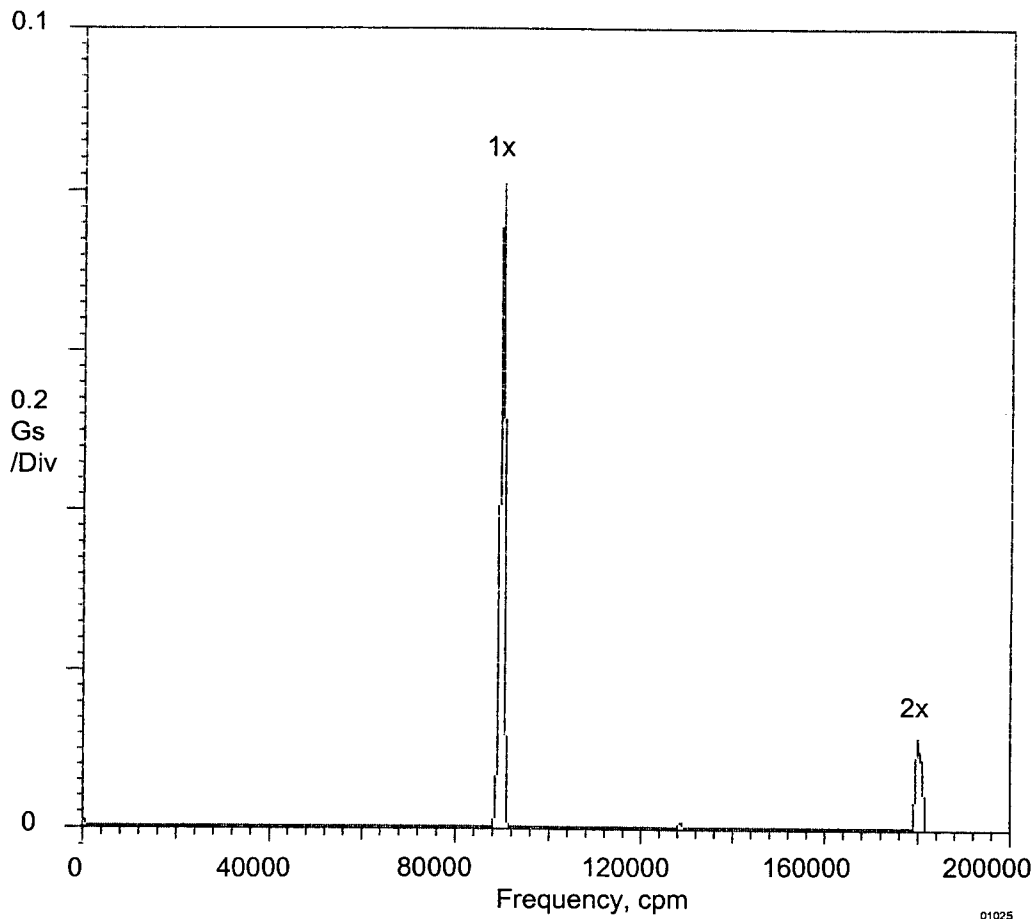


Figure 25. Steady-State Vibration Frequency Spectra at 90,000 rpm for Replacement Bearing

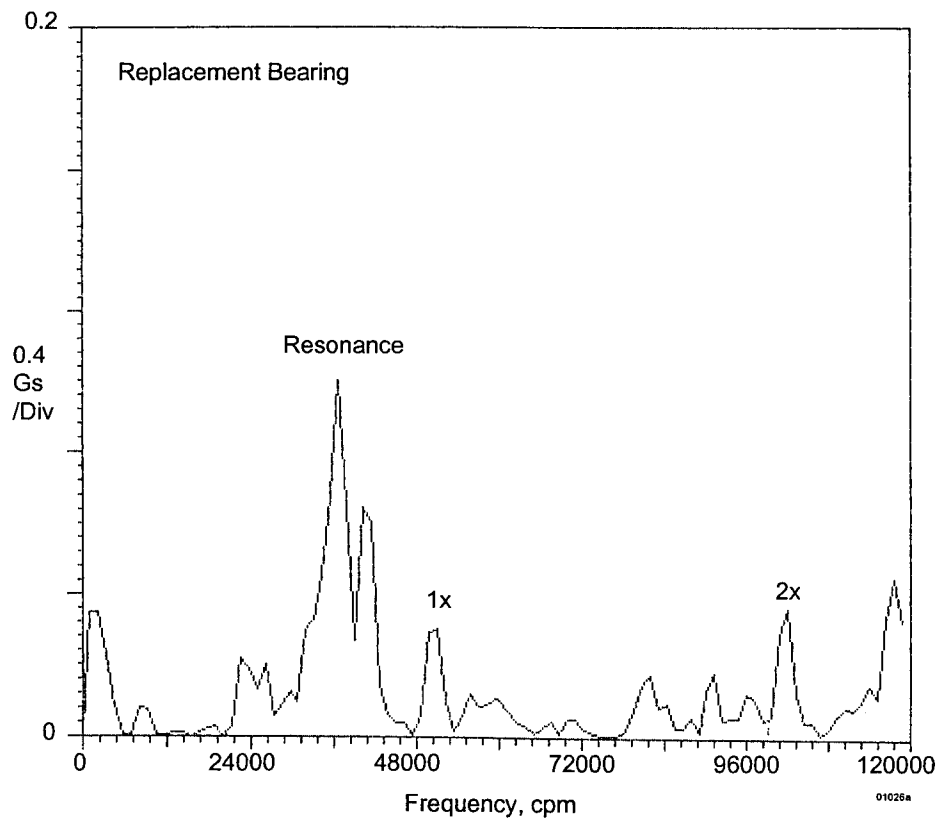
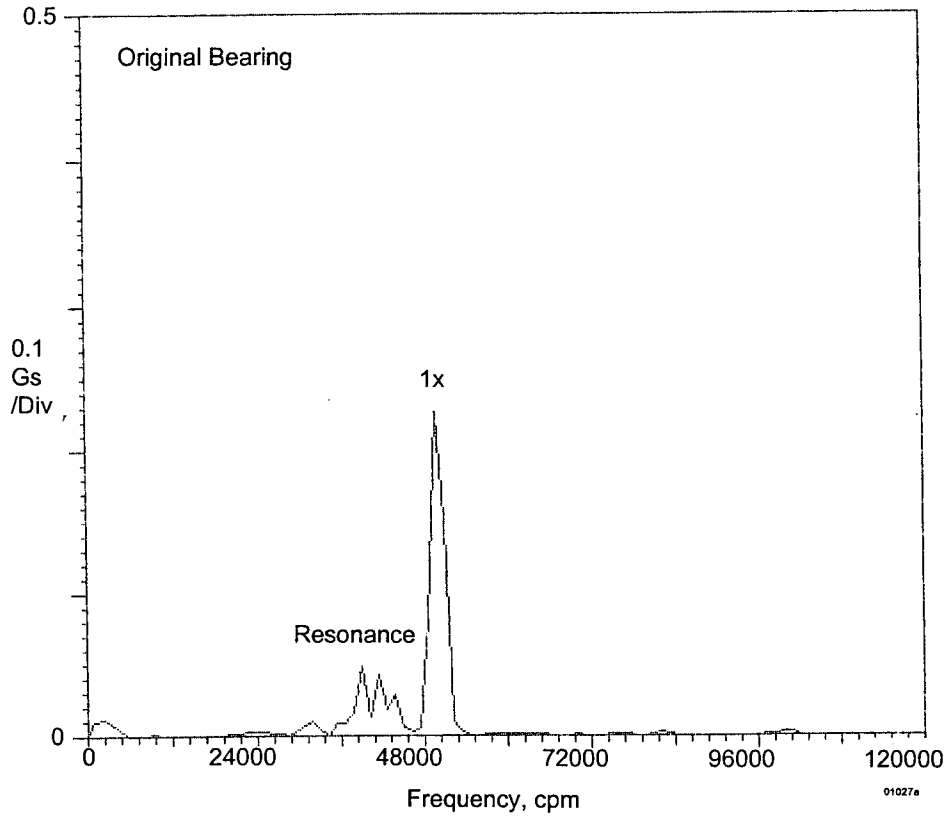


Figure 26. Typical Bearing Response during Shaker Tests